UNIVERSITY OF LEEDS

This is a repository copy of *Conjugate Heat Transfer Computational Fluid Dynamic Predictions of Impingement Heat Transfer: The Influence of Hole Pitch to Diameter Ratio X/D at Constant Impingement Gap Z*.

White Rose Research Online URL for this paper:
http://eprints.whiterose.ac.uk/105021/

Version: Accepted Version

Article:
El-Jummah, AM, Husain, RAAA, Andrews, GE orcid.org/0000-0002-8398-1363 et al. (1 more author) (2014) Conjugate Heat Transfer Computational Fluid Dynamic Predictions of Impingement Heat Transfer: The Influence of Hole Pitch to Diameter Ratio X/D at Constant Impingement Gap Z. Journal of Turbomachinery, 136 (12). 121002. ISSN 0889-504X

https://doi.org/10.1115/1.4028232

Reuse
Items deposited in White Rose Research Online are protected by copyright, with all rights reserved unless indicated otherwise. They may be downloaded and/or printed for private study, or other acts as permitted by national copyright laws. The publisher or other rights holders may allow further reproduction and re-use of the full text version. This is indicated by the licence information on the White Rose Research Online record for the item.

Takedown
If you consider content in White Rose Research Online to be in breach of UK law, please notify us by emailing eprints@whiterose.ac.uk including the URL of the record and the reason for the withdrawal request.

White Rose university consortium
Universities of Leeds, Sheffield & York

eprints@whiterose.ac.uk
https://eprints.whiterose.ac.uk/

Journal of Turbomachinery. Received July 07, 2014;
Accepted manuscript posted August 11, 2014. doi:10.1115/1.4028232
Copyright (c) 2014 by ASME

Conjugate Heat Transfer CFD Predictions of Impingement Heat Transfer: The Influence of Hole Pitch to Diameter Ratio X/D at Constant Impingement Gap Z

A. M. El-Jummah[1]

Energy Research Institute

School of Chemical and Process Engineering

University of Leeds

Leeds LS2 9JT, UK

al-jummah@hotmail.com

ASME No. 100277595

R. A. A. Abdul Husain

Energy Research Institute

School of Chemical and Process Engineering

University of Leeds

Leeds LS2 9JT, UK

mnamej@leeds.ac.uk

G. E. Andrews

Energy Research Institute

School of Chemical and Process Engineering

University of Leeds

Leeds LS2 9JT, UK

profgeandrews@hotmail.com

J. E. J. Staggs

Energy Research Institute

School of Chemical and Process Engineering

University of Leeds

Leeds LS2 9JT, UK

J.E.J.Stagggs@leeds.ac.uk

[1] Corresponding Author

Accepted Manuscript Not Copyedited

Downloaded From: http://turbomachinery.asmedigitalcollection.asme.org/ on 08/11/2014 Terms of Use: http://asme.org/terms

Journal of Turbomachinery. Received July 07, 2014;
Accepted manuscript posted August 11, 2014. doi:10.1115/1.4028232
Copyright (c) 2014 by ASME

ABSTRACT

Conjugate heat transfer (CHT) computational fluid dynamic (CFD) predictions, were carried out for a 10 × 10 square array of impingement holes, for a range of pitch to diameter ratio X/D from 1.9 to 11.0 at a constant impingement gap Z of 10mm and pitch X of 15.24mm. The variation of X/D changes the impingement wall pressure loss for the same coolant mass flow rate and also changes the interaction with the impingement gap cross-flow. The experimental technique to determine the surface averaged heat transfer used the lumped capacity method with Nimonic-75 metal walls with imbedded thermocouples and a step change in the hot wall cooling to determine the heat transfer coefficient h from the transient cooling of the metal wall. The test wall was electrically heated to about 80^{o}C and then transiently cooled by the impingement flow and the lumped capacitance method was used to measure the locally surface average heat transfer coefficient. The predictions and measurements were carried out at an impingement jet mass flux of 1.93kg/sm^{2}bar, which is a typical coolant flow rate for regenerative impingement cooling of low NOx gas turbine combustor walls. The computations were conducted for a fixed hot side temperature of 353K that was imposed at the hot face of the target wall. The wall temperatures as a function of distance along the gap were computed together with the impingement gap aerodynamics. Surface average heat transfer coefficient h and pressure loss predictions were in good agreement with the experimental measurements. However, there was less good agreement for the axial variation of the local surface averaged h for lower values of X/D. The surface averaged heat transfer to the impingement jet wall was also computed and shown to be roughly 70% of target wall impingement heat transfer.

INTRODUCTION

Conjugate heat transfer (CHT) computational fluid dynamic (CFD) predictions, were carried out for a 10 × 10 square array of impingement holes, for a range of pitch to diameter ratio X/D from 1.9 to 11.0 at a constant impingement gap Z of 10mm and pitch X of 15.24mm. The variation of X/D changes the impingement wall pressure loss for the same coolant mass flow rate and also changes the interaction with the impingement gap cross-flow. The experimental technique to determine the surface averaged heat transfer, used the lumped capacity method with Nimonic-75 metal walls with imbedded thermocouples and

Accepted Manuscript Not Copyedited

Downloaded From: http://turbomachinery.asmedigitalcollection.asme.org/ on 08/11/2014 Terms of Use: http://asme.org/terms

Journal of Turbomachinery. Received July 07, 2014;
Accepted manuscript posted August 11, 2014. doi:10.1115/1.4028232
Copyright (c) 2014 by ASME

a step change in the hot wall cooling to determine the heat transfer coefficient h from the transient cooling of the metal wall. The test wall was electrically heated to about 80^{o}C and then transiently cooled by the impingement flow and the lumped capacitance method was used to measure the locally surface average heat transfer coefficient. The predictions and measurements were carried out at an impingement jet mass flux of 1.93kg/sm^{2}bar, which is a typical coolant flow rate for regenerative impingement cooling of low NOx gas turbine combustor walls. The computations were conducted for a fixed hot side temperature of 353K that was imposed at the hot face of the target wall. The wall temperatures as a function of distance along the gap were computed together with the impingement gap aerodynamics. Surface average heat transfer coefficient h and pressure loss predictions were in good agreement with the experimental measurements. However, there was less good agreement for the axial variation of the local surface averaged h for lower values of X/D. The surface averaged heat transfer to the impingement jet wall was also computed and shown to be roughly 70% of target wall impingement heat transfer.

The important design variables in impingement cooling are as shown in Fig. 2, which are the pitch to diameter ratio X/D, impingement gap to diameter ratio Z/D, the number of holes per surface area n and the number of holes N, in the direction of the cross-flow in the impingement gap. There are currently insufficient experimental data to enable optimum impingement cooling designs to be developed, particularly for the regeneratively cooled wall case [7]. The use of conjugate heat transfer (CHT) computational fluid dynamics (CFD) can enable optimum impingement air hole configurations to be developed for particular applications [4, 5, 8].

The problem with impingement cooling with no associated effusion film cooling is that the efflux of the cooling air along the gap produces a cross-flow [9 - 11]. This cross-flow deteriorates the heat transfer with distance along the gap and may induce a flow-maldistribution in the rows of impingement holes. Figure 3 shows that if $P_1 - P_2$ (low mass flow rate) < $P_1 - P_2$ (high mas flow rate) implies cross-flow and if $P_3 - P_2 > P_1 - P_2$ then flow-maldistribution is severe. Flow-maldistribution is influenced by the X/D and the number of upstream rows of holes N [9 - 11]. The present work investigates experimentally and using CHT CFD the influence of X/D. The experimental results were for metal walls with active conjugate heat transfer and

Accepted Manuscript Not Copyedited

Downloaded From: http://turbomachinery.asmedigitalcollection.asme.org/ on 08/11/2014 Terms of Use: http://asme.org/terms

Journal of Turbomachinery. Received July 07, 2014;
Accepted manuscript posted August 11, 2014. doi:10.1115/1.4028232
Copyright (c) 2014 by ASME

thus provided data to validate the CHT CFD methodology, so that it could be used more generally in gas turbine cooling system design.

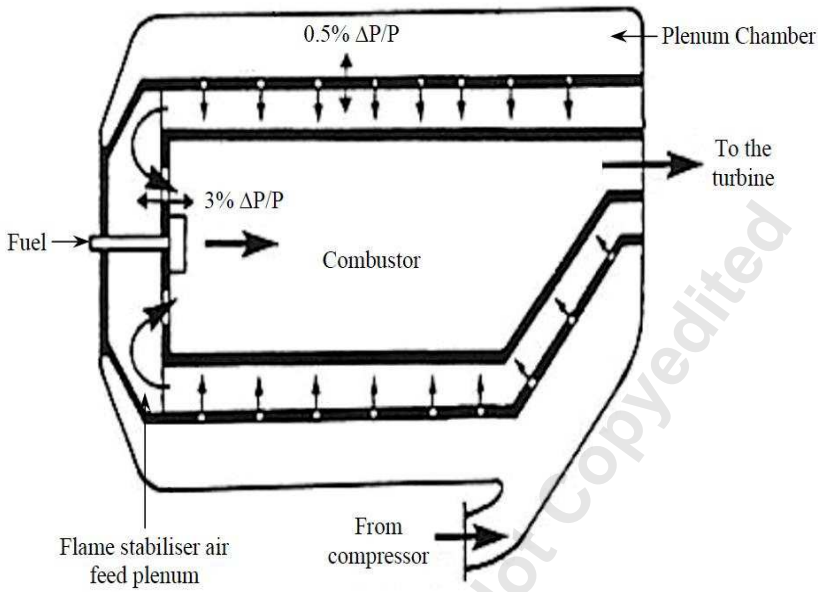

Fig. 1: Schematic of regenerative cooled combustor

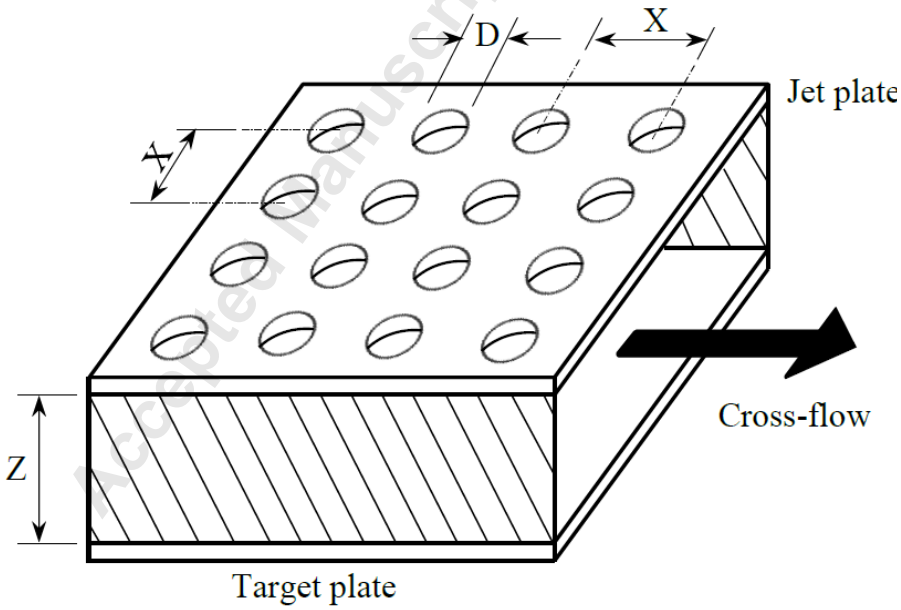

Fig. 2: Impingement jet cooling geometrical setup

Accepted Manuscript Not Copyedited

Downloaded From: http://turbomachinery.asmedigitalcollection.asme.org/ on 08/11/2014 Terms of Use: http://asme.org/terms

Journal of Turbomachinery. Received July 07, 2014;
Accepted manuscript posted August 11, 2014. doi:10.1115/1.4028232
Copyright (c) 2014 by ASME

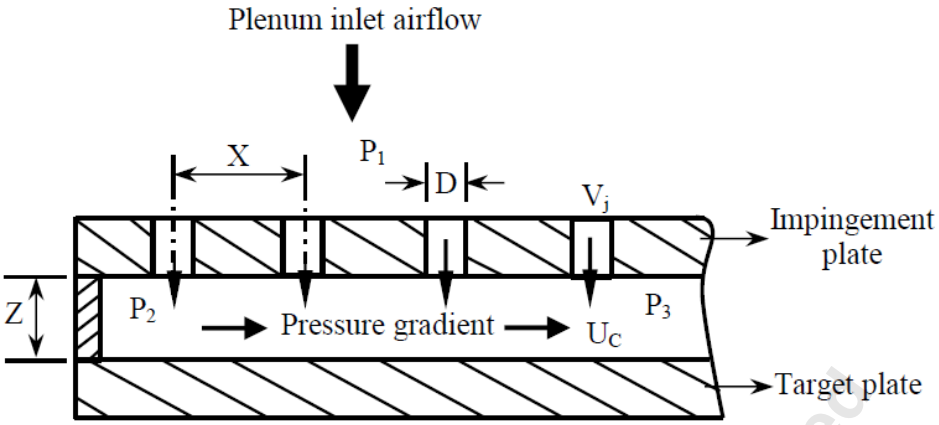

Fig. 3: Schematic diagram of impingement jet cooling geometrical setup with gap cross-flow pressure gradient [7].

Conductive heat transfer in the metal wall occurs in practical engines, but most experimental and CFD investigations of impingement heat transfer are for adiabatic wall conditions. The issue of the design of impingement systems in terms of the number of holes and the optimum X/D are not amenable to design from current correlations. Essentially the optimum impingement cooling design for a fixed Z, is for the lowest number of rows of holes N and the largest X/D that can be tolerated without excessive thermal gradients in the metal wall. This cannot be determined from experiments with adiabatic walls. Essentially the thermal gradients will determine the number of holes and the maximum pitch X allowable and this will determine the optimum number of holes. The authors have shown that the n = 4306m^{-2} used in the present work was close to the optimum X for an X/D of 4.7 [19]. The present work was carried out to investigate the influence of X/D at a constant n of 4306m^{-2}

Effects of X/D on Impingement Heat Transfer

The pitch to diameter ratio X/D can be varied by varying X at constant D, which changes n and the pressure loss or D at constant X. This keeps n constant, as the pressure loss is varied and this was the method of varying X/D used in the present work and in previous experimental work using four sided exit impingement cooling [12, 13]. Whichever method of varying X/D is used, the main associated effect is to vary the impingement jet velocity V_j and impingement wall pressure loss $\Delta P/P$ as the total impingement air

Accepted Manuscript Not Copyedited

Downloaded From: http://turbomachinery.asmedigitalcollection.asme.org/ on 08/11/2014 Terms of Use: http://asme.org/terms

Journal of Turbomachinery. Received July 07, 2014;
Accepted manuscript posted August 11, 2014. doi:10.1115/1.4028232
Copyright (c) 2014 by ASME

flow porosity A is varied. This is shown by Eqs. 1 - 3 for square array impingement holes. Increasing X/D increases V_j at constant G and this increases the impingement heat transfer.

$$\frac{X}{D}=\left(\frac{\pi}{4A}\right)^{0.5} \tag{1}$$

$$G=\frac{V_j A}{RT}=C_d A\left(\frac{2}{RT}\frac{\Delta P}{P}\right)^{0.5} \tag{2}$$

$$V_j=\frac{G}{\rho A}=\frac{4G}{\pi\rho}\left(\frac{X}{D}\right)^2=C_d\left(2RT\frac{\Delta P}{P}\right)^{0.5} \tag{3}$$

Several investigators have shown that increasing X/D or open area porosity A, enhances the heat transfer [14] due to the increased impingement jet velocity and associated turbulence levels. For geometries with large X/D and small A, Eqs. 1 - 3 show that for a given coolant mass flux G, the pressure loss will increase. If the impingement gap Z is constant, then the pressure loss of the cross-flow along the gap does not vary significantly with X/D. This is because the cross-flow velocity U_c is fixed by G and Z, as shown by Eq. 4. However, Eq. 5 shows that as the impingement jet velocity increases with X/D, then the ratio of V_j to the cross-flow velocity V_j/U_c increases. This assumes that the two flow densities are the same, which is valid in the present low temperature experiments. If X/D is large enough and there is no flow-maldistribution between the rows of impingement jet holes in the cross-flow direction, then heat transfer deteriorates with distance from the first row of holes [3, 14 -17]. This effect was correlated by Chance [14] and Kercher and Tabakoff [15] using the term I_c as in Eq. 6.

$$U_c=\frac{NG(X/Z)}{\rho} \tag{4}$$

$$\frac{V_j}{U_c}=\left[\left(\frac{1}{N}\right)\left(\frac{4}{\pi}\right)\left(\frac{X}{D}\right)^2\left(\frac{Z}{X}\right)\right]=\left[\frac{Z}{NAX}\right] \tag{5}$$

$$\frac{Nu}{Nu_o}=1-0.2361I_C=1-0.236\left(\frac{G_C}{G}\right)\left(\frac{Z}{D}\right) \tag{6}$$

Accepted Manuscript Not Copyedited

Downloaded From: http://turbomachinery.asmedigitalcollection.asme.org/ on 08/11/2014 Terms of Use: http://asme.org/terms

Journal of Turbomachinery. Received July 07, 2014;
Accepted manuscript posted August 11, 2014. doi:10.1115/1.4028232
Copyright (c) 2014 by ASME

$$\frac{Nu}{Nu_o} = 1 - 0.188\frac{ND}{X} = 1 - 0.188\left(\frac{WD}{X^2}\right) \qquad (7)$$

Where W is the length of wall to be cooled.

Andrews and Hussain [10, 11] showed that Eq. 6 could be shown to be converted to Eq. 7, if the density of the cross-flow and impingement jet were the same. This shows that the deterioration of the heat transfer with distance along the gap is not dependent on the gap depth, which is an unexpected result, first noticed by Chance [14] and Gaunter et al. [21]. To minimize the deterioration of heat transfer for a length of wall to be cooled, Eq.7 shows the importance of using a large X or a small N with a small D. How large X can be made will depend on the thermal gradients in the wall, which this present work investigates. Equations 1 - 7 assumes equal coolant flow distribution to each impingement hole.

A further feature of impingement cooling with single sided exit from the impingement gap is that the pressure loss generated by the cross-flow generates a flow-maldistribution for low impingement wall pressure loss. Equations 2 and 3 show that at constant G, the impingement wall pressure loss reduces as X/D reduces or A increases. Thus, at low X/D the pressure loss along the cross-flow direction is significant relative to the impingement wall pressure loss and flow-maldistribution occurs with the downstream impingement holes receiving more air [15]. Andrews and Hussain [10, 11], showed using Eq. 8 that flow-maldistribution could be predicted for incompressible jet flow by the ratio G_N/G_1, derived from the ratio 'y' of jet to cross-flow pressure loss as in Eq. 9.

$$y = \left(\frac{Z}{C_d NAX}\right)^2 \qquad (8)$$

$$\frac{G_N}{G_1} = \sqrt{\left[\frac{y}{1-y}\right]} \qquad (9)$$

Equations 8 and 9 show that if 'y' is large then the flow-maldistribution will be large. Decreasing Z or increasing N, A or X will make the flow-maldistribution increase. In the present work the hole porosity A was varied by varying D at constant X. Previously, El-Jummah et al. [5] have used CHT CFD to explore

Accepted Manuscript Not Copyedited

Downloaded From: http://turbomachinery.asmedigitalcollection.asme.org/ on 08/11/2014 Terms of Use: http://asme.org/terms

Journal of Turbomachinery. Received July 07, 2014;
Accepted manuscript posted August 11, 2014. doi:10.1115/1.4028232
Copyright (c) 2014 by ASME

the consequences of varying Z at constant X, D, N and A. Strong flow-maldistribution was shown for X/D = 4.7 at low Z/D, which was minimal at high Z/D.

EXPERIMENTAL TECHNIQUES

The experimental equipment [1, 7 - 13] is as shown in Fig. 4a. It consists of an air supply to a thermally insulated plenum chamber feed to the impingement holes. Nimonic-75 impingement test plates, shown in Fig. 4b of 152.4mm square were bolted to the plenum chamber. An impingement gap Z of 10mm was set using a Teflon spacer flange which formed a one sided exit channel. The Teflon spacer has a low thermal conductivity and this minimized the transfer of heat between the two metal walls. Nimonic-75 is a common combustor metal wall material which was the reasons for its choice as the target wall.

Figure 4b shows the schematic diagram of the test plates with the location of the imbedded grounded junction mineral insulated thermocouples shown. The thermocouples were brazed to the Nimonic-75 walls with the thermocouple junction flush with the impingement jet target surface. There were six thermocouples at 25.4mm intervals placed on the centreline between the impingement surface jets and thus at the most remote places relative to the high local convective cooling of the impingement points. Conductive heat transfer within the wall smoothed out the strong gradients in surface convective heat transfer, as the Biot numbers for all conditions were < 0.2. The thermocouples thus measured a surface averaged temperature and were located at the lowest local convective heat transfer position and hence would give slightly higher temperatures than the mean and thus result in conservative heat transfer measurements.

In addition to the central thermocouples, Fig. 4b shows that on the target wall there were thermocouples located 25.4mm either side of the centre line. These were used to determine the transverse variation of the surface averaged heat transfer h. The variability between these thermocouples was the principle error in the determination of h. This error was due to the experimental variability in the hole diameter due to manufacturing tolerances, which produced a variation in coolant mass flow rates per hole. In addition to the hole diameter variation the hole inlet and internal surface roughness were variable due to manufacturing tolerances. The variation in the thermocouple response between the three and five transverse

Accepted Manuscript Not Copyedited

Downloaded From: http://turbomachinery.asmedigitalcollection.asme.org/ on 08/11/2014 Terms of Use: http://asme.org/terms

Journal of Turbomachinery. Received July 07, 2014;
Accepted manuscript posted August 11, 2014. doi:10.1115/1.4028232
Copyright (c) 2014 by ASME

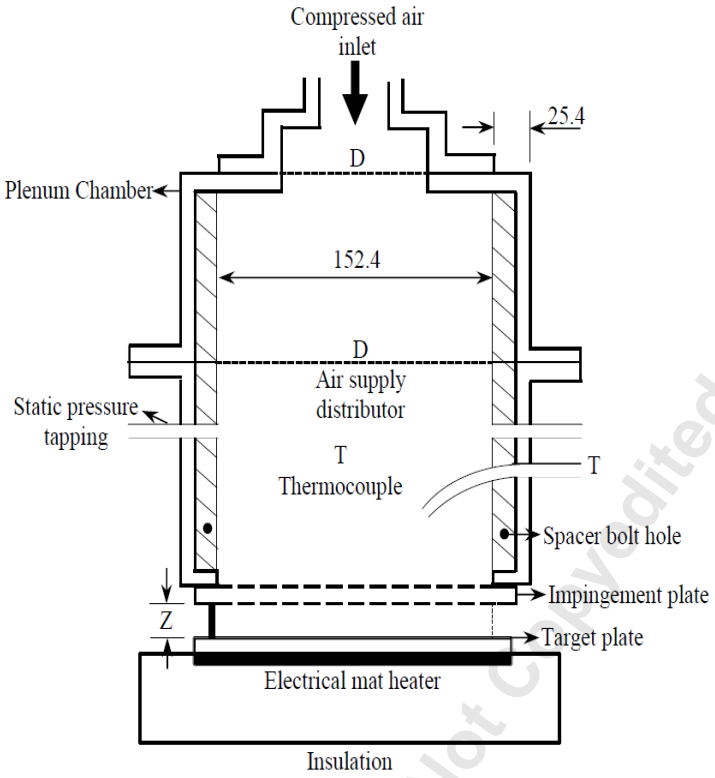

a) Test rig

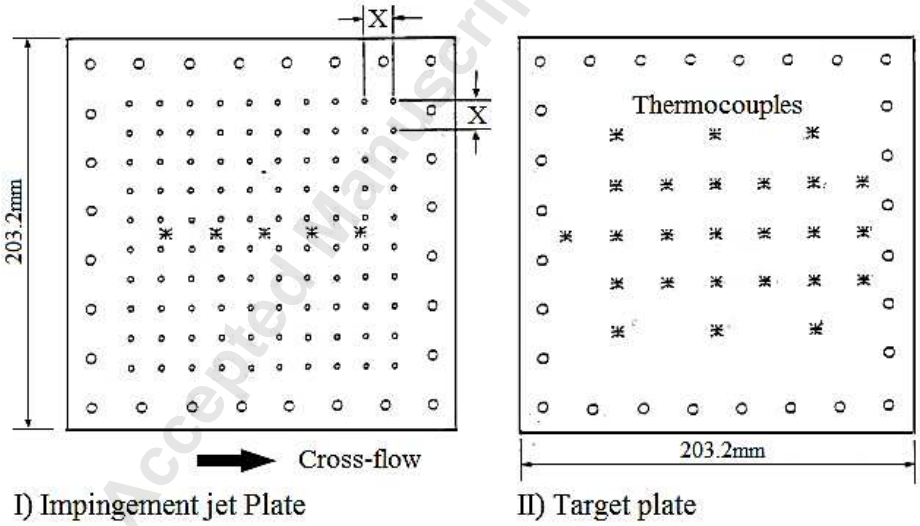

b) Test plates

Fig. 4: Impingement cooling experimental test rig and test plates configurations with thermocouples locations

Downloaded From: http://turbomachinery.asmedigitalcollection.asme.org/ on 08/11/2014 Terms of Use: http://asme.org/terms

Journal of Turbomachinery. Received July 07, 2014;
Accepted manuscript posted August 11, 2014. doi:10.1115/1.4028232
Copyright (c) 2014 by ASME

thermocouples in Fig. 4b was 5% and this was used as the accuracy of the measurements of h.

$$h = \frac{q''}{(T_s - T_\infty)} \qquad (10)$$

The target wall thermocouples were used to determine the locally surface averaged heat transfer coefficient using the lumped capacitance method [1, 7 - 3]. The thermally insulated wall was electrically heated in the absence of any impingement coolant flow to about 80^{o}C and then the electrical heating was switched off, after which the impingement flow was established. The transient cooling of the target wall by the impingement flow enabled the surface averaged heat transfer coefficient to be determined using Eq. 10 [5, 18]. Abdul-Husain and Andrews [7] have shown that this method gave good agreement with steady state methods of heat transfer measurements [14, 15, 17] for the same impingement geometry and air hole Reynolds number. In their work, comparison was also made between steady state and transient cooling h for single thermocouples for a range of G values and the results were in agreement.

Table 1 shows the impingement square array geometries that were investigated experimentally and computationally predicted. These are actual size practical combustor wall cooling geometries. Each air hole diameter was measured using a calibrated conical insert micrometre and the air hole size was the average of all the 100 holes. The coolant flow rate was measured using calibrated variable area flow meters with corrections for the air temperature and pressure. The accuracy relative to a calibrated orifice plate flow meter was 2%.

Table 1: Geometrical Parameters

X/D	11.04	6.54	4.66	3.78	3.06	1.86
D (mm)	1.38	2.33	3.27	4.03	4.98	8.18
X (mm)	15.24	15.24	15.24	15.24	15.24	15.24
Z (mm)	10.0	10.0	10.0	10.0	10.0	10.0
L (mm)	6.35	6.35	6.35	6.35	6.35	6.35
L/D	4.60	2.73	1.94	1.58	1.28	0.78
Z/D	7.25	4.29	3.06	2.48	2.01	1.22
X/Z	1.52	1.52	1.52	1.52	1.52	1.52
A%	0.64	1.84	3.62	5.50	8.39	22.7
n (m^{-2})	4306	4306	4306	4306	4306	4306
Array	10 × 10	10 × 10	10 × 10	10 × 10	10 × 10	10 × 10

Accepted Manuscript Not Copyedited

Downloaded From: http://turbomachinery.asmedigitalcollection.asme.org/ on 08/11/2014 Terms of Use: http://asme.org/terms

Journal of Turbomachinery. Received July 07, 2014;
Accepted manuscript posted August 11, 2014. doi:10.1115/1.4028232
Copyright (c) 2014 by ASME

COMPUTATIONAL METHODS

Grid Generation

Previously, El-Jummah et al. [8] carried out CHT CFD investigations for a range of G (kg/sm^{2}bar) using symmetrical representation (Fig. 5a) of one row of impingement holes, the same procedure was applied in modelling the present grid geometries using the ANSYS ICEM meshing tool. The model grid with all the component parts is shown in Fig. 5 and for each X/D half hole size, the grids are shown in Fig. 6. The cell size 'ξ' in the holes and the impingement gap was varied because of the differences in hole sizes D and Reynolds number Re. The total model grid size of Fig. 5 is shown in Table 2 for each X/D. These gave maximum grid aspect ratios and orthogonal qualities of the cells for all the geometries in the range of 1.78 - 7.58 and 0.59 - 0.61, respectively.

Figure 6 shows that for each air hole size, the cell size varies, which will be shown later to influence the flow characteristics in the hole. In each air hole, the number of cells/plane ranges from 60 to 95 (twice for complete hole) and this was determined by the hole size D, the higher D the larger the number of cells in each plane. For each air hole, 18 grid planes were fixed and this was held constant for all the geometries. As the jet size decreased, the grid size in the impingement gap increased and this influenced the number of cells in the gap. Hence, an X/D of 11.04 has the highest number of cells with X/D of 1.86 having the lowest. This brings about the total number of cells in all the grid geometries to within the range of 1.0 - 2.0 million as shown in Table 2, where X/D = 11.04 has the highest number of cells.

Model computations

The present CFD work was computed using the standard k - ε turbulence model with the standard wall function in the ANSYS Fluent code [4, 5, 8, 18, 19]. The effect of other turbulence models have been investigated but are not reported here, as none gave better agreement with the experimental results. The problem with all the other turbulence models available in Fluent was that they could not predict the flow separation and reattachment that occurred in the impingement jet holes. As a consequence none could

Accepted Manuscript Not Copyedited

Downloaded From: http://turbomachinery.asmedigitalcollection.asme.org/ on 08/11/2014 Terms of Use: http://asme.org/terms

Journal of Turbomachinery. Received July 07, 2014;
Accepted manuscript posted August 11, 2014. doi:10.1115/1.4028232
Copyright (c) 2014 by ASME

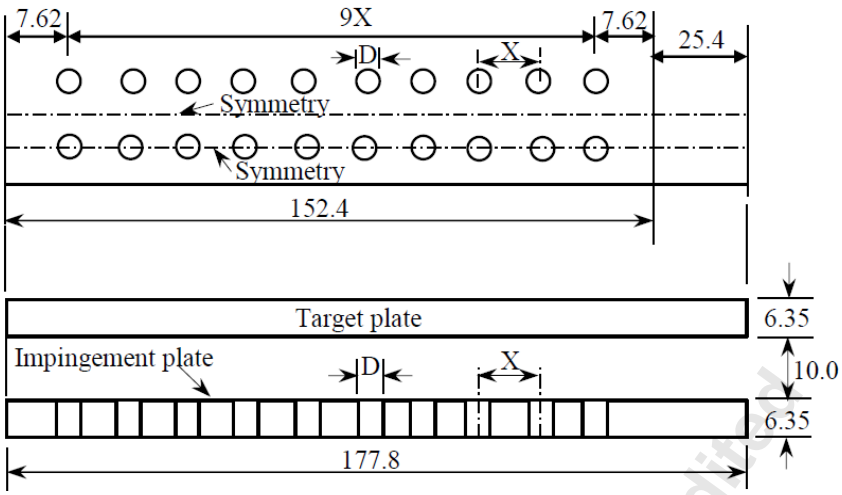

Not to scale and all dimensions in mm.

(a) Symmetrical elements

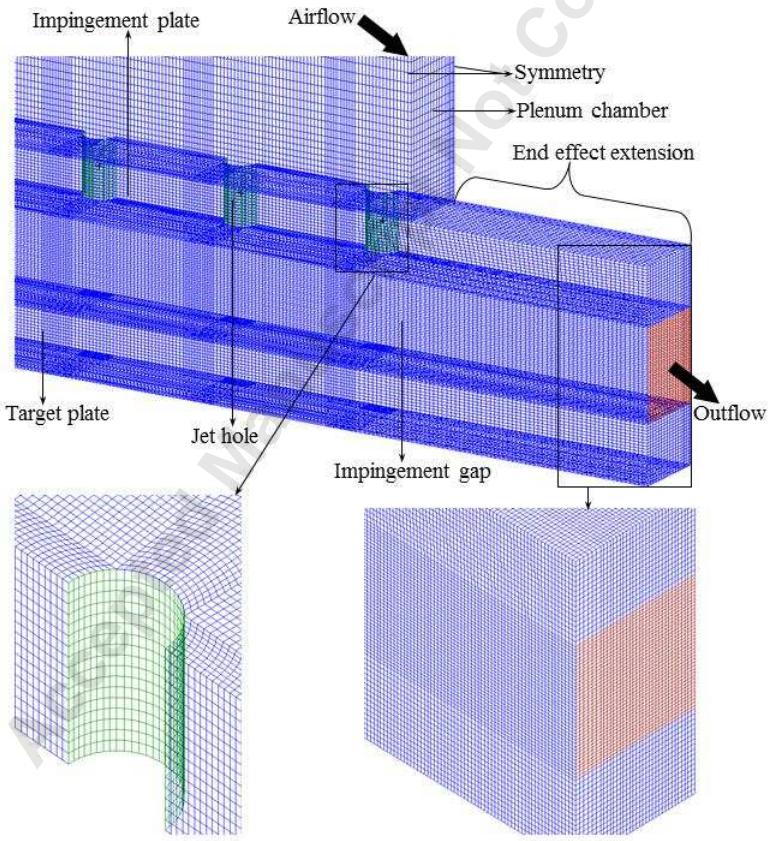

(b) Model grids

Fig. 5: Impingement cooling computational domain

Downloaded From: http://turbomachinery.asmedigitalcollection.asme.org/ on 08/11/2014 Terms of Use: http://asme.org/terms

Journal of Turbomachinery. Received July 07, 2014;
Accepted manuscript posted August 11, 2014. doi:10.1115/1.4028232
Copyright (c) 2014 by ASME

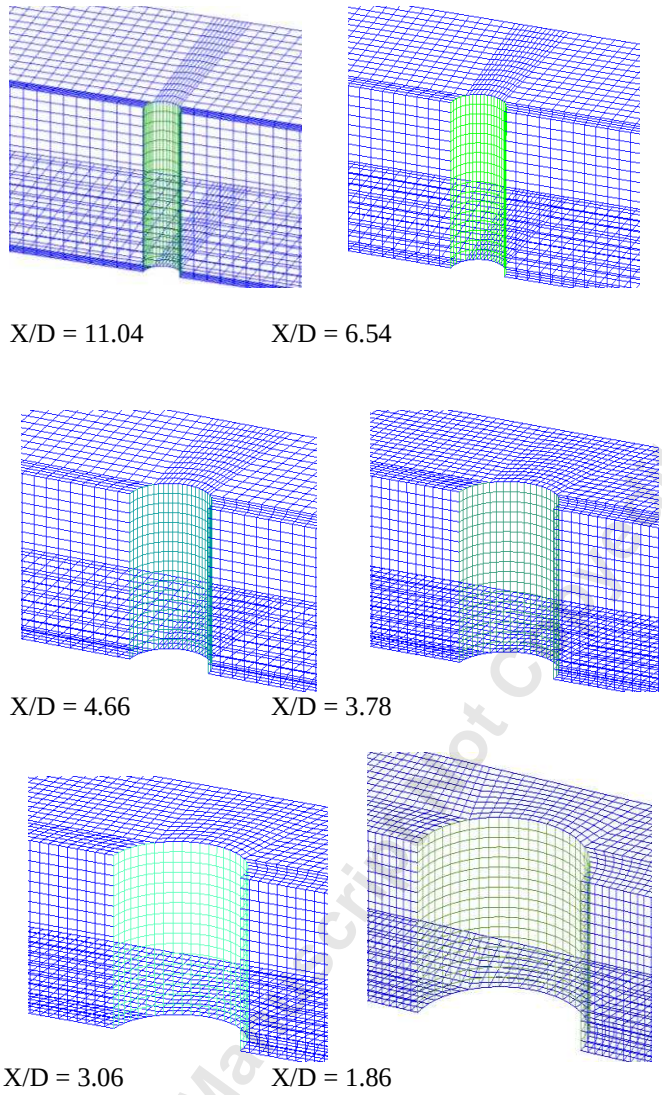

Fig. 6: Grid impingement cooling air holes for variable X/D and D (mm) at constant X of 15.24mm

Table 2: Grid Size and y^+ used for Geometries in Table 1

X/D	Total	Plenum (%)	Gap (%)	Hole (%)	y^+
11.04	2.08×10^6	31.4	45.9	7.1	44.8
6.54	1.77×10^6	35.7	33.6	6.6	39.2
4.66	1.27×10^6	37.6	27.8	6.1	35.9
3.78	1.14×10^6	42.0	21.7	4.8	35.6
3.06	1.06×10^6	46.5	19.2	4.9	34.9
1.86	0.98×10^6	48.2	14.9	8.8	34.2

correctly predict the measured pressure loss, which is controlled by the flow separation at the hole inlet. None of the models, including the SST k - ω, could predict the flow reattachment adequately and this

Downloaded From: http://turbomachinery.asmedigitalcollection.asme.org/ on 08/11/2014 Terms of Use: http://asme.org/terms

Journal of Turbomachinery. Received July 07, 2014;
Accepted manuscript posted August 11, 2014. doi:10.1115/1.4028232
Copyright (c) 2014 by ASME

results in the hole outlet velocity profile being too high in the centre, which resulted in the inter-gap aerodynamics being predicted to be quite different than for the k - ε turbulence model.

The first cell size near the target wall was maintained at a y^+ value of ~ 40 for X/D ranging from 1.86 - 6.54, but for X/D = 11.04 the y^+ value was ~ 45 which was used to reduce the total number of cells (~ 2.0×10^6) and hence computational time/cost [18, 20 - 23]. Table 2 shows the range of y^+ values and their respective grid size. These y^+ values are within the required range for the near wall law of the wall; $30 < y^+ < 300$ [5, 8, 18, 21]. The choice of the y^+ values was based on the closer link [21, 22] that they gave between the turbulence or log-log layer and the target wall. Hence, the heat transfer characteristics were easily determined. These choices of y^+ values also helped to minimize the total number of cells as the same first cell sizes were employed throughout the impingement gap. Since the computations for low Reynolds number models with y^+ of ~ 1 or ~ 5 takes longer [18, 21] and do not adequately resolve the short hole entry length issues [21], the choice of the present y^+ value was preferred.

Table 3: Flow Parameters at Fixed G of 1.93kg/sm^{2}bar

X/D	11.04	6.54	4.66	3.78	3.06	1.86
$\mathbf{V_j}$ (m/s)	243.60	85.49	43.41	28.56	18.72	6.92
$\mathbf{U_c}$ (m/s)	23.92	23.92	23.92	23.92	23.92	23.92
$\mathbf{V_j/U_c}$	10.18	3.57	1.82	1.19	0.78	0.29
N	10	10	10	10	10	10
$\mathbf{Re_h}$	22870	13550	9660	7830	6340	3850
$\mathbf{T_\infty}$ (K)	288	288	288	288	288	288
$\mathbf{T_w}$ (K)	353	353	353	353	353	353
$\boldsymbol{\rho}$ (kg/m^3)	1.225	1.225	1.225	1.225	1.225	1.225

Grid independence tests were previously investigated [4, 5] and the present number of cells in the hole and along the impingement gap was found to be adequate, which is good in predicting the experimental data. This will be shown later to agree with experimental pressure loss and surface averaged heat transfer coefficient predictions in the present work, hence within the experimental errors [24, 25]. The boundary conditions used for each computation are shown in Table 3. The convergence criteria were set at 10^{-5} for continuity, 10^{-11} for energy and 10^{-7} for k, ε and momentum (x, y and z velocities), respectively.

Accepted Manuscript Not Copyedited

Downloaded From: http://turbomachinery.asmedigitalcollection.asme.org/ on 08/11/2014 Terms of Use: http://asme.org/terms

Journal of Turbomachinery. Received July 07, 2014;
Accepted manuscript posted August 11, 2014. doi:10.1115/1.4028232
Copyright (c) 2014 by ASME

Previous Work on CHT CFD in Gas Turbines

This work present experimental results and CHT CFD predictions using hot metal walls for classic impingement cooling geometries. Most work in the literature on impingement cooling uses adiabatic heat transfer techniques [14 - 18, 20, 21]. There is a dearth of experimental data to compare and validate CHT CFD predictions. Some researches on this topic in gas turbines have no experimental validation due to this lack of hot rig metal wall experimental data [26 - 28]. Sometimes inappropriate wall materials are used, such as Aluminium [29], so that there are no thermal gradients to predict. The use of radiation based wall temperature measurents in hot test rigs can result in poor agreement with CHT CFD, possibly due to emissivity calibration problems, as the emissivity is a function of temperature [30, 31]. When imbedded thermocouples are used as in the present work, there is a growing body of evidence, particularly for metal turbine blade studies of agreement between CHT CFD predictions and metal temperature measurements [32, 33]. For flat wall effusion cooling Oguntade et al. [34 - 36], have shown good agreement with experimental hot test result for Nimonic-75 effusion walls with imbedded thermocouples.

RESULTS

Influence of X/D on Flow Maldistribution

The ratio of the flow through hole row 10 and row 1 is the flow-maldistribution. The predicted flow-maldistribution between the 10 rows of impingement holes using Eq. 9 is shown in Table 4. Flow-maldistribution was predicted to be large for X/D > 4.7. The CFD predictions of the flow-maldistribution were made based on the mean velocity in each hole at the midpoint of the hole length, which is shown as a ratio to the mean hole velocity based on equal mass flow distribution between the holes, given as V_j in Table 3. The predictions from Fig. 7 at hole 10 are compared with those from Eq. 9 in Table 4.

The X/D of 4.66 is at the limit of the condition where flow-maldistribution between the holes starts to become a significant problem [7 - 11]. Table 4 shows that the simple 1D flow-maldistribution theory of Eqs. 8 and 9 is increasingly in error with excessive flow-maldistribution predicted, as X/D was reduced compared with the CFD predictions. The reason for this is that it has been assumed in the simple theory

Accepted Manuscript Not Copyedited

Downloaded From: http://turbomachinery.asmedigitalcollection.asme.org/ on 08/11/2014 Terms of Use: http://asme.org/terms

Journal of Turbomachinery. Received July 07, 2014;
Accepted manuscript posted August 11, 2014. doi:10.1115/1.4028232
Copyright (c) 2014 by ASME

that the outlet velocity profile of each hole was not influenced by the cross-flow and that the impingement gap has its full area available for cross-flow. But the impingement jets block the cross-flow and this blockage gets greater as X/D reduces or D increases. This increases the pressure loss of the cross-flow as well as causing more jet deflection. However, the main effect is that of the cross-flow on the hole outlet velocity profile, which has been shown in detail for one geometry by El-Jummah et al. [4]. The cross-flow produces a peak in the hole outlet velocity profile to the downward edge of the hole. This increases the hole pressure loss for the downstream holes and this reduces the mass flow through that hole and thus reduces the flow-maldistribution predicted using 1D theory which ignores these effects. Thus the flow-maldistribution is lower at low X/D in the CFD predictions compared with the predictions of Eq. 9, as shown in Table 4.

In the present work, the Z/D ratio changes with reduced X/D as Z was held constant. For an X/D of 4.66 El-Jummah et al. [5] predicted the influence of Z/D, the impact of this on the flow-maldistribution is shown in Fig. 8, which shows a very small difference of Z/D at an X/D of 4.66. Thus, the big change in flow-maldistribution for an X/D of 1.86 at a Z/D of 1.22 predicted in this work was due to the X/D effect and not the Z/D effect. This is because, a Z/D of 1.3 and X/D of 4.66 were shown to have the same flow-maldistribution difference, as for Z/D of 3.06 and X/D of 4.66. This was also predicted by Eqs. 8 and 9, respectively.

Table 4: CFD and 1D Predicted Flow-maldistribution

X/D	CFD	Equation 9
11.04	0.96	1.04
6.54	1.04	1.12
4.66	1.09	1.29
3.78	1.14	1.44
3.06	1.30	1.59
1.86	2.49	3.55

Accepted Manuscript Not Copyedited

Downloaded From: http://turbomachinery.asmedigitalcollection.asme.org/ on 08/11/2014 Terms of Use: http://asme.org/terms

Journal of Turbomachinery. Received July 07, 2014;
Accepted manuscript posted August 11, 2014. doi:10.1115/1.4028232
Copyright (c) 2014 by ASME

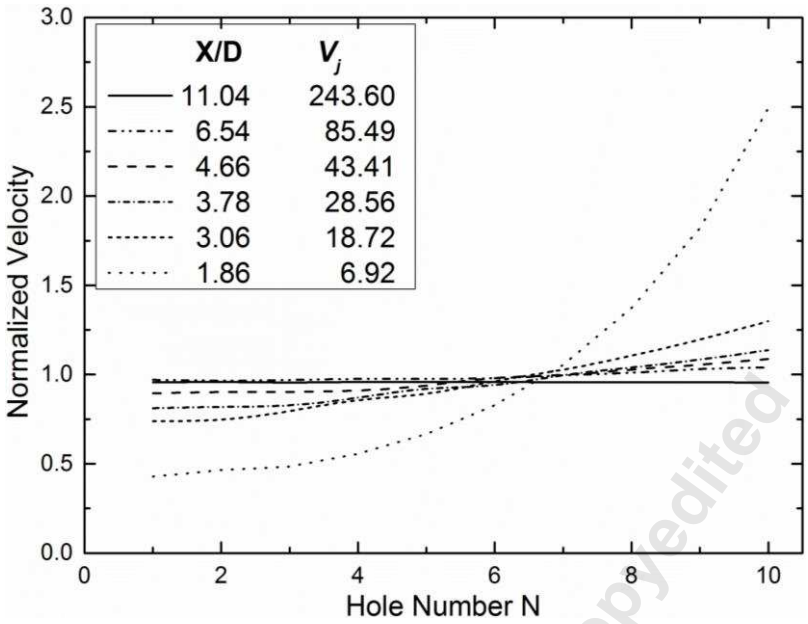

Fig. 7: Flow-maldistribution in the impingement plate holes for variable X/D and constant G of 1.93kg/sm^{2}bar

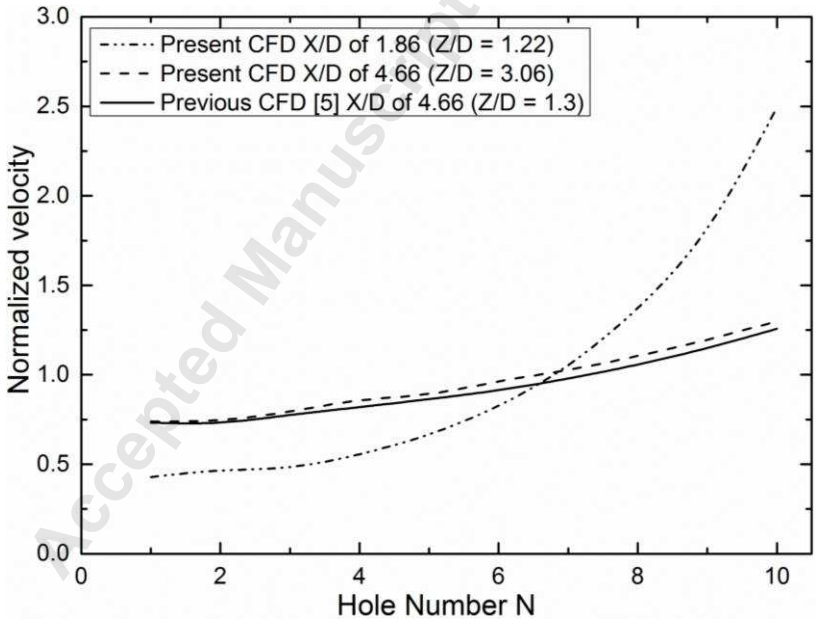

Fig. 8: Comparison of predicted flow-maldistribution with previous CFD prediction showing influence of Z/D

Downloaded From: http://turbomachinery.asmedigitalcollection.asme.org/ on 08/11/2014 Terms of Use: http://asme.org/terms

Journal of Turbomachinery. Received July 07, 2014;
Accepted manuscript posted August 11, 2014. doi:10.1115/1.4028232
Copyright (c) 2014 by ASME

Predicted Velocity Profiles and Pressure Loss

Figure 9 shows the predicted velocity profiles in the impingement gap for the range of X/D, at constant G of 1.93kg/sm^{2}bar. A plane on the centreline of the jets and a plane on the centreline between the jets are shown, these are the symmetry planes shown in Fig. 5. Figure 9a shows that at an X/D = 11.04, the high velocity impingement jets penetrate to the impingement wall with very little deflection by the cross-flow. This was due to the very high jet to cross-flow velocity ratio that was shown by Eq. 5 for large X/D or low impingement jet wall porosity A. As X/D decreases and A increases, Fig. 9 shows that there is deflection of the downstream jets by the cross-flow. At low X/D, Fig. 9b shows that the deflection by the cross-flow is predicted to be severe and also the flow-maldistribution is clear with the last hole having a higher velocity than the first hole.

Figure 9 also shows that on the centreline between the impingement jets there is a reverse flow jet that impinges on the impingement hole wall between the impingement jets. There is a strong reverse jet at large X/D and this weakens as X/D is reduced and the impingement jet velocity decreases. This reverse flow jet is deflected by the cross-flow and this deflection is greater at low X/D. These predicted impingement jet aerodynamics were investigated in more detail for one impingement geometry by El-Jummah et al. [4]. The impingement jet velocity and the aerodynamics of the flow inside the holes, controls the pressure loss [19]. The CFD predictions enable the pressure loss through the impingement jet wall and that along the impingement gap due to the cross-flow to be determined. The predicted pressure loss is the static pressure in the air supply plenum chamber minus the static pressure at the impingement jet wall on the centre point between the impingement jets. This predicted pressure loss as a % of the static upstream pressure is shown in Fig. 10, as a function of the axial distance along the impingement gap in terms of the number of holes. Equations 2 and 3 show the strong link between the pressure loss and X/D and the impingement wall porosity A. Thus at high X/D of 11.04, the pressure loss at the high coolant mass flux G of 1.9kg/sm^{2}bar was predicted to be very high which is at an unrealistic level for gas turbine applications. This is because an X/D of 11.04 would not be used with all the compressor flow. It is the design choice for local hot spot

Accepted Manuscript Not Copyedited

Downloaded From: http://turbomachinery.asmedigitalcollection.asme.org/ on 08/11/2014 Terms of Use: http://asme.org/terms

Journal of Turbomachinery. Received July 07, 2014;
Accepted manuscript posted August 11, 2014. doi:10.1115/1.4028232
Copyright (c) 2014 by ASME

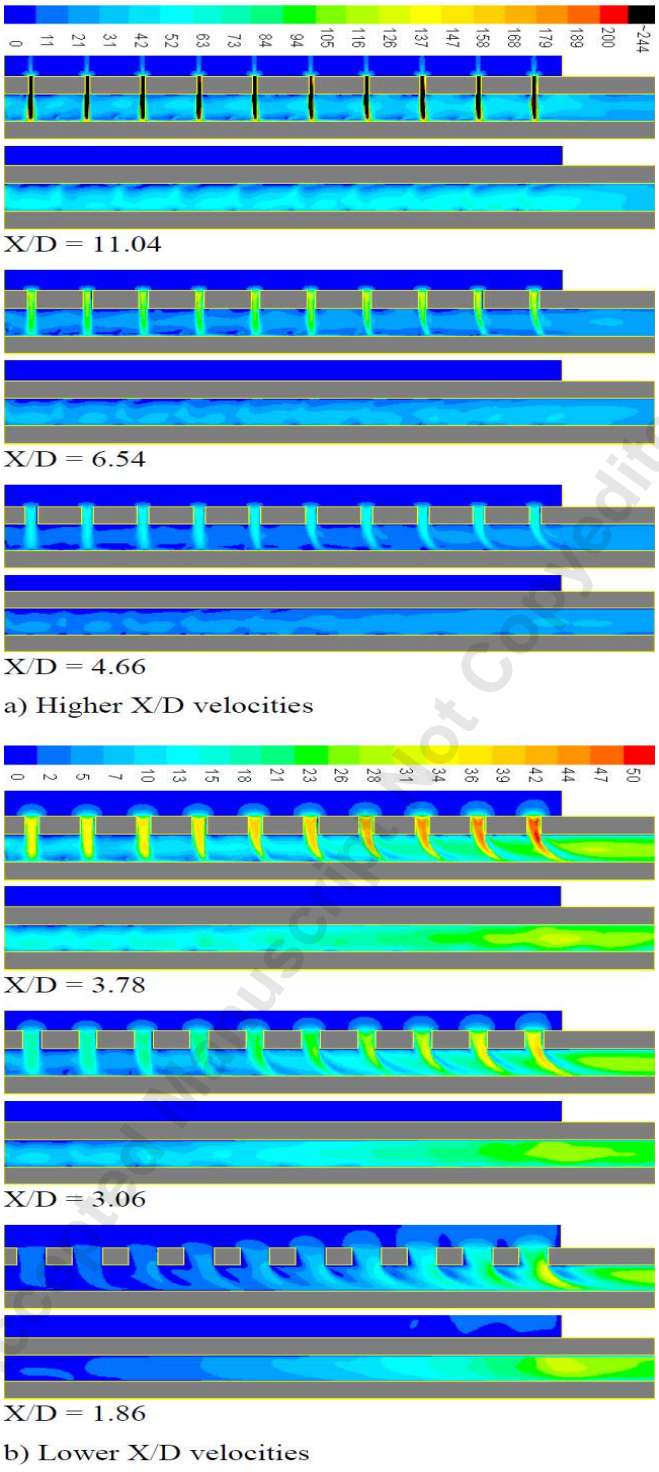

Fig. 9: Contours of velocity magnitude (m/s) in the impingement gap (in line with and between rows of holes) for variable X/D. Grey colour stripes are Nimonic-75 walls

Downloaded From: http://turbomachinery.asmedigitalcollection.asme.org/ on 08/11/2014 Terms of Use: http://asme.org/terms

Journal of Turbomachinery. Received July 07, 2014;
Accepted manuscript posted August 11, 2014. doi:10.1115/1.4028232
Copyright (c) 2014 by ASME

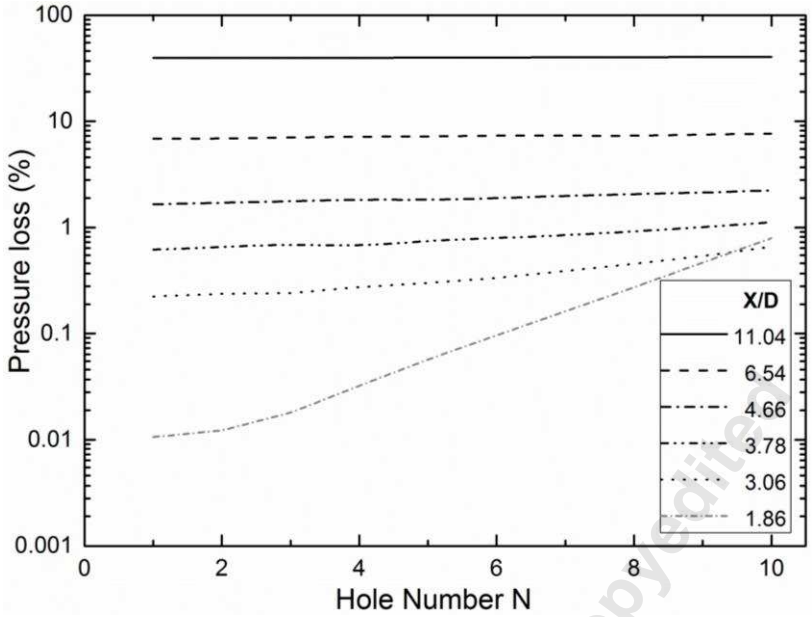

Fig.10: Predictions of outlet impingement holes pressure loss for variable X/D at constant G of 1.93kg/sm^{2}bar

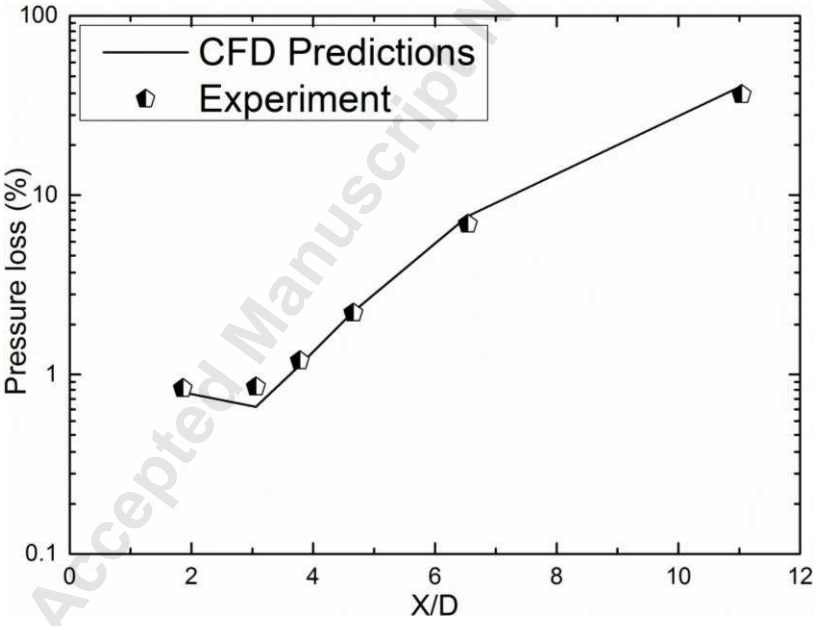

Fig.11: Comparison of predicted pressure loss with experiment for range of X/D at constant G of 1.93kg/sm^{2}bar

Accepted Manuscript Not Copyedited

Downloaded From: http://turbomachinery.asmedigitalcollection.asme.org/ on 08/11/2014 Terms of Use: http://asme.org/terms

Journal of Turbomachinery. Received July 07, 2014;
Accepted manuscript posted August 11, 2014. doi:10.1115/1.4028232
Copyright (c) 2014 by ASME

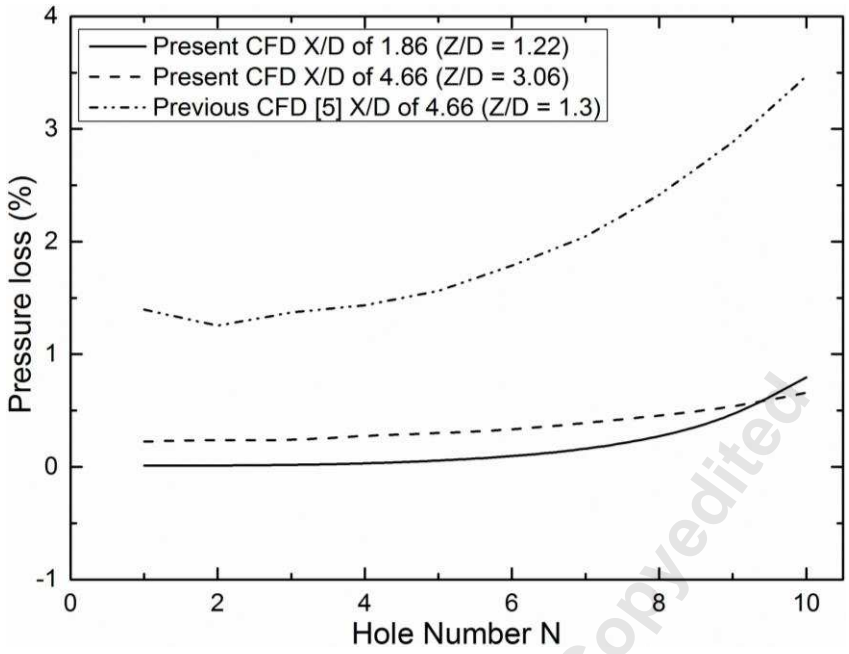

Fig.12: Comparison of predicted pressure loss with Previous CFD prediction showing influence of Z/D

cooling of combustor walls or turbine blades, where a small proportion of the total compressor air flow is used but at a low local G with a 3 - 4% pressure loss. However, the variation of X/D at constant mass flux was the objective of the present CFD investigation.

Figure 10 show that the pressure loss along the cross-flow gap was predicted to be small relative to the impingement jet wall pressure loss at high X/D. However, as X/D is reduced and the pressure loss reduces, the cross-flow pressure loss becomes more significant, especially for X/D < 3.78. It is in this region that the flow-maldistribution becomes significant as shown in Fig. 7. The pressure loss was experimentally measured as the static pressure difference between the plenum chamber and the external ambient air. This was then corrected for the small pressure loss of the cross-flow discharge from the impingement gap. This was computed as one dynamic head pressure loss, based on the mean impingement gap flow U_c in Table 3. This correction was 0.34% and was the same for all X/D. The CFD predictions did not predict the pressure loss of the dump expansion from the gap and predicted the pressure loss to the upstream wall static pressure 25.4mm downstream of the last row of impingement holes. The predicted pressure loss is compared with the measured pressure loss in Fig. 11, this shows very good agreement at all X/D. The pressure loss is the

Accepted Manuscript Not Copyedited

Downloaded From: http://turbomachinery.asmedigitalcollection.asme.org/ on 08/11/2014 Terms of Use: http://asme.org/terms

Journal of Turbomachinery. Received July 07, 2014;
Accepted manuscript posted August 11, 2014. doi:10.1115/1.4028232
Copyright (c) 2014 by ASME

only measured parameter that is directly related to the flow aerodynamics. However, the pressure loss cannot be predicted if the flow separation in the impingement holes is not adequately predicted. Thus agreement of the predicted pressure loss with the measurements shows that the predicted aerodynamics in the impingement hole and gap are likely to be reliable. This was not the case for other turbulence models that were investigated.

The present work was carried out at a constant impingement gap Z, so that the cross-flow velocity was the same irrespective of the X/D. However, this did involve a change in Z/D as D was increased at constant X in this work. Figure 12 compares the predicted pressure loss in the present work with that investigated by El-Jummah et al. [5], who varied Z/D at constant X/D of 4.66 in a CHT CFD predictions, using the same procedures as in the present work and was part of the present investigations. Figure 12 shows that at similar Z/D of 1.2 - 1.3 the influence of increased X/D at near constant Z/D was to increase the pressure loss substantially, as shown by Eqs. 2 and 3.

Predicted Turbulent Kinetic Energy Distribution

The turbulent kinetic energy (TKE) on the impingement target wall controls the convective heat transfer. The predicted target surface distribution of TKE is shown in Fig. 13. The peak turbulence lies below the impingement point of the jet and there is low turbulence at the reverse flow jet position on the wall. The peak turbulence decreases as X/D is decreased due to the associated reduction in peak impingement jet velocities for the same mass flux. Figure 13 also shows the impact of the cross-flow on the target surface turbulence distribution. This is negligible at an X/D of 11.04, but becomes increasingly significant as X/D is reduced. Figure 13 shows that at an X/D of 4.66 or below the convection of the turbulence downstream of the impingement point is an increasing feature of the effect of cross-flow. Also, the flow-maldistribution starts to increase the peak turbulence in the downstream portion of the cross-flow at low X/D.

Accepted Manuscript Not Copyedited

Downloaded From: http://turbomachinery.asmedigitalcollection.asme.org/ on 08/11/2014 Terms of Use: http://asme.org/terms

Journal of Turbomachinery. Received July 07, 2014;
Accepted manuscript posted August 11, 2014. doi:10.1115/1.4028232
Copyright (c) 2014 by ASME

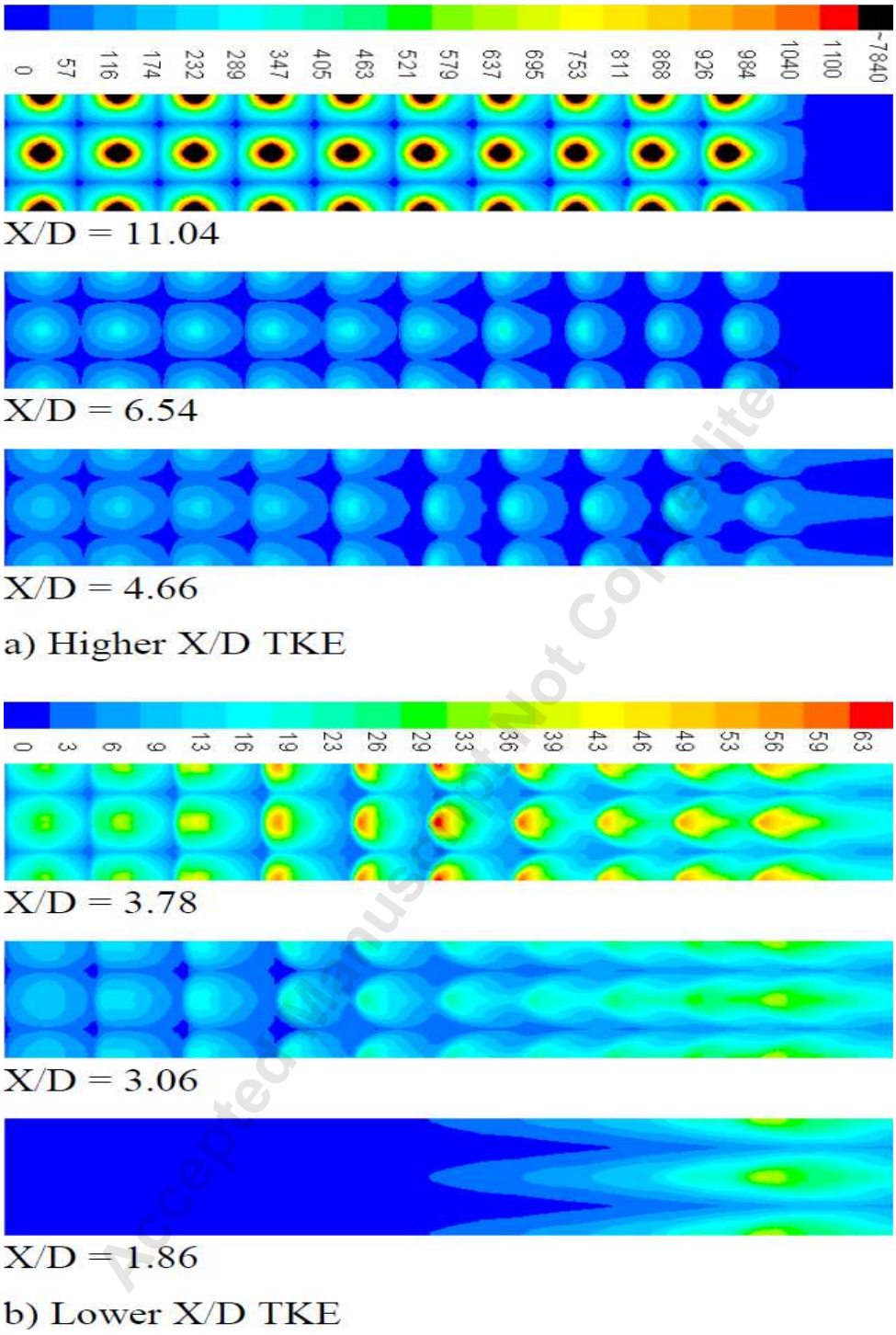

Fig. 13: Contours of TKE (m^2/s^2) on the target wall surface for variable X/D at constant G of 1.93kg/sm^2bar

Downloaded From: http://turbomachinery.asmedigitalcollection.asme.org/ on 08/11/2014 Terms of Use: http://asme.org/terms

Journal of Turbomachinery. Received July 07, 2014;
Accepted manuscript posted August 11, 2014. doi:10.1115/1.4028232
Copyright (c) 2014 by ASME

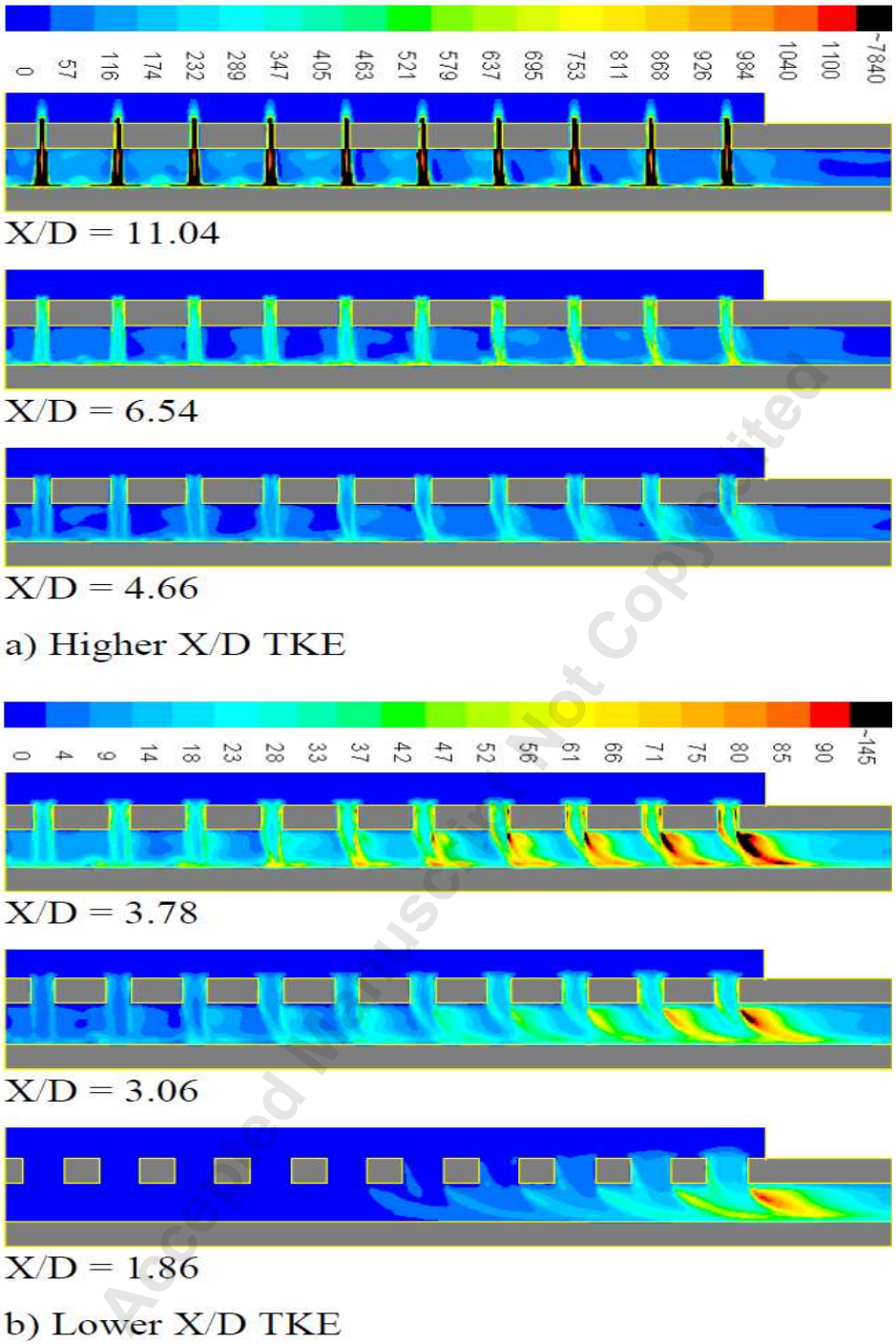

Fig. 14: Contours of TKE (m^2/s^2) in the impingement gap in-line with the jet for variable X/D at constant G. Grey colour stripes are Nimonic-75 walls

Downloaded From: http://turbomachinery.asmedigitalcollection.asme.org/ on 08/11/2014 Terms of Use: http://asme.org/terms

Journal of Turbomachinery. Received July 07, 2014;
Accepted manuscript posted August 11, 2014. doi:10.1115/1.4028232
Copyright (c) 2014 by ASME

The TKE in the gap in-line with the jets is shown in Fig. 14. This shows that a major action of the cross-flow is to convect the high turbulence shear layer downstream around the jet and this effect increases as X/D is reduced. The action of the cross-flow prevents the impingement jets from flowing upstream on the surface and thus there is no surface flow impingement between the surface jet flows, which reduces the creation of turbulence on the surface.

The turbulence inside the impingement holes occurs as a result of the pressure loss through the holes and hence the good prediction of the measured pressure loss, shown in Fig. 11 means that the internal hole turbulence levels must be predicted reliably. Figure 15 shows the predicted internal hole surface TKE distribution for the first two and last two holes. The hole surface is shown as the normalised circumference in the bottom scale and hole length in the vertical scale, for which all the holes had the same depth. If there was no significant effect of the cross-flow on the flow in the hole, then the turbulence on the hole surface would be symmetrical. This is the case for an X/D of 11 for all four holes shown in Fig. 15, but becomes increasingly unsymmetrical for the downstream two holes at lower X/D, where the cross-flow is deflecting the jet hole surface turbulence inside the hole. The air entry to the holes separates on the inlet edge and reattaches inside the hole. The peak turbulence on the hole surface occurs at the flow reattachment point. Other turbulence models could not predict the flow separation and reattachment inside the holes and had the greatest discrepancy with the k - ε turbulence model in the hole surface TKE distribution. The heat transfer inside the holes is controlled by the surface turbulence distribution and intensity, as will be shown later.

Surface Averaged Predicted Nusselt Number

The predicted and measured heat transfer coefficients, as defined in Eq. 10, were converted into Nusselt number Nu, by Eq. 11. The predicted surface Nu distribution is shown in Fig. 16 for the target surface (top) and impingement jet surface (bottom) for the range of X/D investigated.

$$Nu = \frac{hD}{k_f} \qquad (11)$$

Accepted Manuscript Not Copyedited

Downloaded From: http://turbomachinery.asmedigitalcollection.asme.org/ on 08/11/2014 Terms of Use: http://asme.org/terms

Journal of Turbomachinery. Received July 07, 2014;
Accepted manuscript posted August 11, 2014. doi:10.1115/1.4028232
Copyright (c) 2014 by ASME

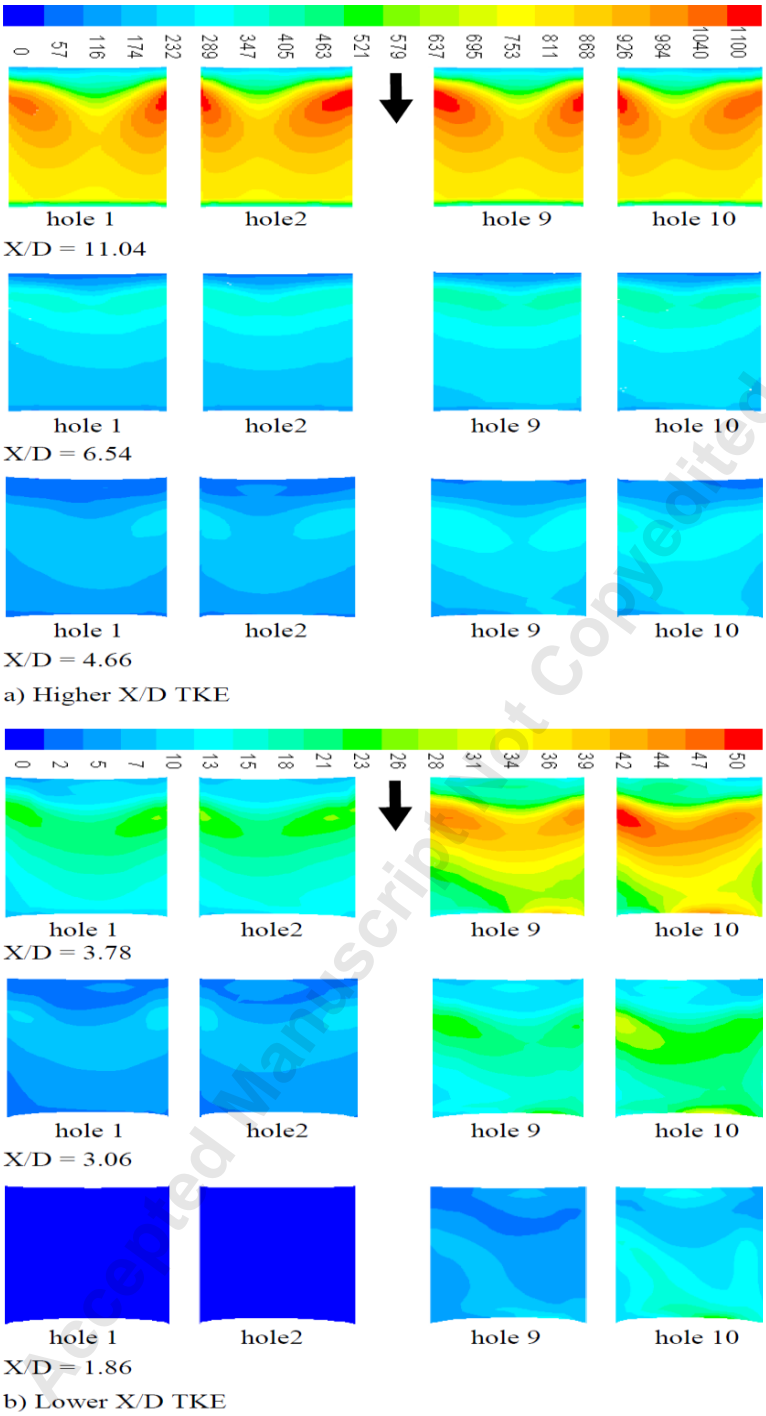

Fig. 15: Contours of TKE (m^2/s^2) on the air hole surface for variable X/D at constant G. Arrow indicates flow direction

Downloaded From: http://turbomachinery.asmedigitalcollection.asme.org/ on 08/11/2014 Terms of Use: http://asme.org/terms

Journal of Turbomachinery. Received July 07, 2014;
Accepted manuscript posted August 11, 2014. doi:10.1115/1.4028232
Copyright (c) 2014 by ASME

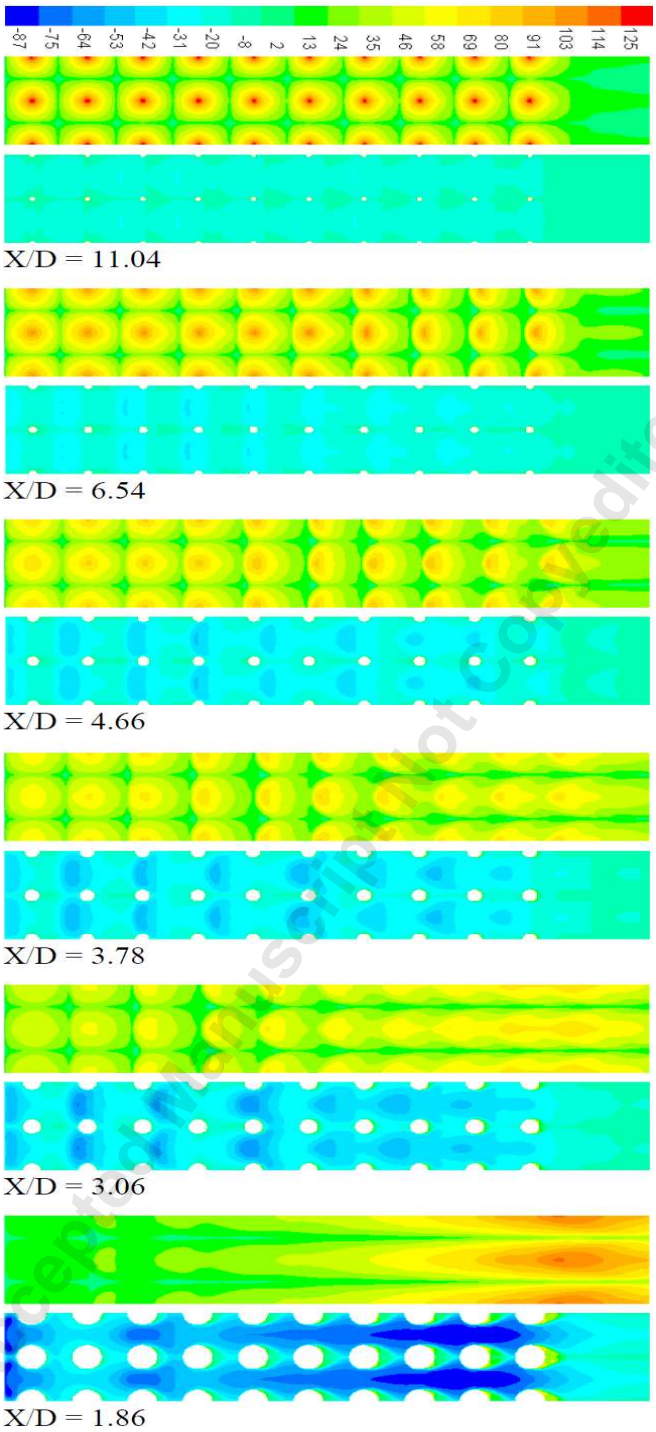

Fig. 16: Contours of Nusselt number on target (top) and inside impingement (bottom) surfaces for variable X/D

Downloaded From: http://turbomachinery.asmedigitalcollection.asme.org/ on 08/11/2014 Terms of Use: http://asme.org/terms

Journal of Turbomachinery. Received July 07, 2014;
Accepted manuscript posted August 11, 2014. doi:10.1115/1.4028232
Copyright (c) 2014 by ASME

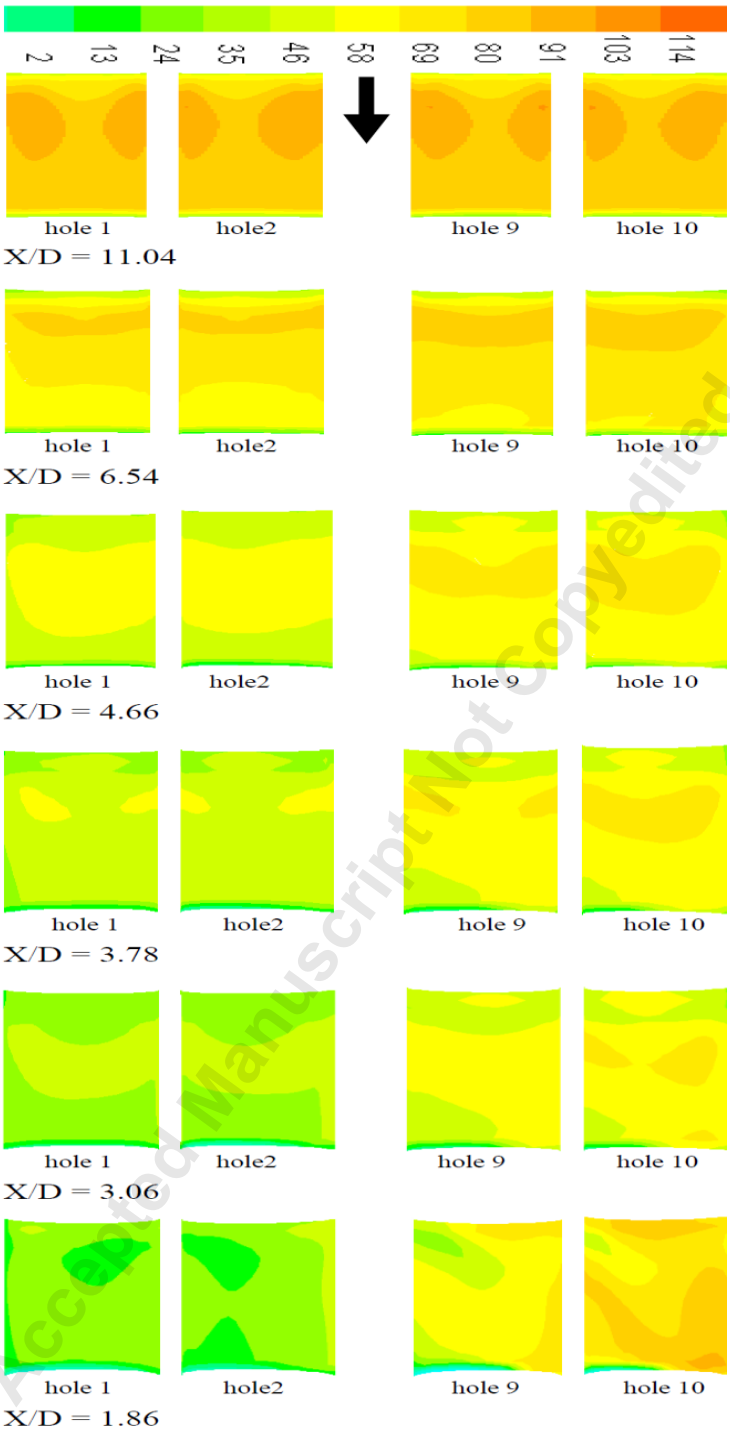

Fig. 17: Contours of Nusselt number on inside impingement hole surfaces for variable X/D at constant mass velocity. The arrow indicates flow direction

Downloaded From: http://turbomachinery.asmedigitalcollection.asme.org/ on 08/11/2014 Terms of Use: http://asme.org/terms

Journal of Turbomachinery. Received July 07, 2014;
Accepted manuscript posted August 11, 2014. doi:10.1115/1.4028232
Copyright (c) 2014 by ASME

Comparison of the Nu distribution on the target surface, with the TKE distribution on the target surface in Fig. 13 shows that the distribution of Nu is controlled by the surface distribution of TKE. These predicted Nu distributions are very similar to the measured surface distributions of h and Nu of Bailey and Bunker [25] and Xing et al. [20] for impingement heat transfer. The spatial distribution of Nu also gives rise to thermal gradients in the target wall. However, the role of the internal wall thermal conduction is to smooth out these gradients, so that the thermal gradients are much lower than the Nu gradients in Fig. 16.

Figure 16 shows that at a high X/D of 11.04, the 10 rows of jets produced nearly identical heat transfer. After the fifth hole the heat transfer distribution starts to distort in the downstream direction due to the action of the cross-flow. This distortion gets worse as X/D decreases and the porosity A increases. At the lowest X/D the individual impingement jets cannot be seen as local regions of high heat transfer and the cross-flow smears the region of high heat transfer in the downstream portion of the test wall. The Nusselt number Nu on the impingement jet surface was also predicted. This heat transfer was caused by the reverse flow jets, discussed above in relation to the predicted aerodynamics in the gap. The heat transfer was lower than on the target wall, but the reverse flow impingement jet can be seen to give a local enhancement of the jet wall heat transfer. This reverse flow heating of the impingement jet wall raises the temperature of that wall, which then heats up the impingement cooling air.

The Nusselt number inside the impingement holes was also predicted and is shown in Fig. 17. Here the normalized circumference is the horizontal axis and the hole depth is the vertical distance. The first two holes in the cross-flow direction are compared with the last two holes. For X/D of 11.04, the hole surface heat transfer was symmetrical indicating no action of the cross-flow. These results should compare with the TKE wall distributions in Fig. 15 as they are similar in their distribution. The peak impingement jet internal wall heat transfer occurs at the inlet flow separated jet reattachment point, where there is a peak in the TKE and Nu. As X/D was reduced the predicted Nu distribution results showed a bias in the hole heat transfer in the cross-flow direction. Also, as flow-maldistribution increased with reduced X/D, Fig. 17 shows that the last 2 holes had significantly higher Nu than the first two holes.

Accepted Manuscript Not Copyedited

Downloaded From: http://turbomachinery.asmedigitalcollection.asme.org/ on 08/11/2014 Terms of Use: http://asme.org/terms

Journal of Turbomachinery. Received July 07, 2014;
Accepted manuscript posted August 11, 2014. doi:10.1115/1.4028232
Copyright (c) 2014 by ASME

Surface Averaged Heat Transfer Coefficient

The X^2 surface average h was computed for each impingement jet and the mean surface average h over all 10 rows of holes is shown in Fig. 18 as a function of X/D. Also shown are the equivalent surface averaged experimental measurements and the agreement is very good and within the experimental error bars for all X/D apart from 1.86. A slightly higher surface averaged heat transfer compared with the measurement was expected, as the measurements used thermocouples located midway between the impingement holes and hence were located in the hottest part of the wall, which would result in lower h if the wall temperature gradients were significant. This is shown in Fig.18 for all X/D apart from X/D of 11.04. The ability of the thermocouples to measure the surface averaged h depends on the Biot number being low. The Biot number decreased with decrease in X/D due to the decrease in h. These effects are shown below in terms of the wall surface temperature gradients.

The under prediction of h for X/D = 1.86 was greater than expected as the Biot number was lowest and the wall would be at a more uniform temperature. The under prediction was possibly influenced by the very low hole Re of 3850, shown in Table 3. This was the mean hole Re, but the flow-maldistribution discussed above, would result in the leading edge hole having a laminar flow of about 1500 Re and hole 10 would be at a Re of about 8500. This is also confirmed by the hole turbulence predictions with zero turbulence predicted at the leading edge holes in Fig.15. Figure 19b shows that the difference in the predictions and measurement were highest at the leading edge. It is concluded that the k - ε turbulence model is not appropriate when portions of the flow are under laminar flow conditions.

The predicted surface averaged h for the impingement jet walls are also shown in Fig. 18. This impingement jet wall heat transfer is due to the transfer of heat by the reverse flow jets discussed above. On average this impingement jet surface averaged h was predicted to be 40% - 60% of that for the impingement target wall at all X/D. However, there were significant variations in this ratio with X/D and between the first few holes and the last few holes. Clearly the heating of the impingement jet wall by the recirculating impingement jets from the hot surface is a significant part of the overall complex heat transfer in impingement cooling. There are no measurements of the heat transfer to this surface to our knowledge and it was not measured in the present work. However, the reasonable agreement of the predicted and

Accepted Manuscript Not Copyedited

Downloaded From: http://turbomachinery.asmedigitalcollection.asme.org/ on 08/11/2014 Terms of Use: http://asme.org/terms

Journal of Turbomachinery. Received July 07, 2014;
Accepted manuscript posted August 11, 2014. doi:10.1115/1.4028232
Copyright (c) 2014 by ASME

measured surface averaged heat transfer indicates that the predictions for the surface averaged impingement jet wall heat transfer could be reasonable. Andrews et al. [12] have measured the heating of the impingement jet wall in a similar test rig to the present, but with four sided impingement flow exit. For a steady state electrically heated target wall the temperature of the impingement wall could be as large as 60% of that of the target wall at low G, high X/D and low Z/D. For low X/D with lower velocity jets, the heating of the impingement jet wall at low G was 30% of the target heated wall temperature. At high G the impingement wall heating decreased, but was still 10 - 20% of the target wall temperature.

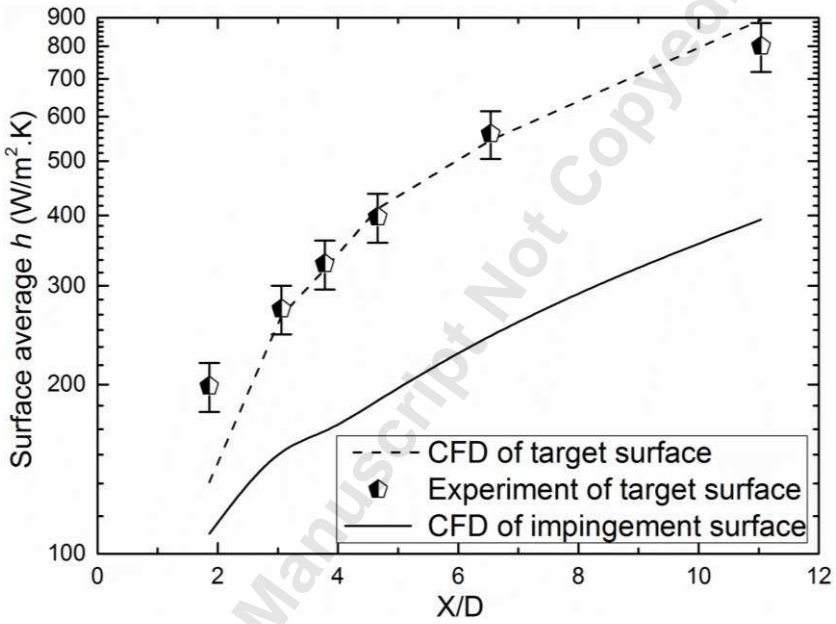

Fig.18: Comparison of target surface average heat transfer coefficient h and prediction of impingement plate HTC h

Axial Variation of the X^2 Local Average HTC

The experimental results had six equispaced thermocouples imbedded in the metal wall. The transient response of these enabled the surface average heat transfer coefficient h, to be determined at the 25.4mm spacing of the thermocouples. The experimental results are shown in Fig. 19 for G = 1.93kg/sm^{2}bar. This shows that for X/D of 11.04, the heat transfer was fairly uniform with a slight increase in the trailing edge region, possible due to the duct flow additional heat transfer of the crossflow. These results indicate that at

Accepted Manuscript Not Copyedited

Downloaded From: http://turbomachinery.asmedigitalcollection.asme.org/ on 08/11/2014 Terms of Use: http://asme.org/terms

Journal of Turbomachinery. Received July 07, 2014;
Accepted manuscript posted August 11, 2014. doi:10.1115/1.4028232
Copyright (c) 2014 by ASME

an X/D of 11.04 the deterioration of heat transfer with distance, as correlated by Eq. 7, does not occur. This supports the prediction of the aerodynamics in Fig. 9, where there was minimal movement of the jets by the cross-flow.

The agreement of the CFD results with the experiments was rather poor for X/D of 11.04, apart from in the leading edge region. The reason for this might be associated with the use of incompressible flow CFD, when at this X/D the jet velocities are very high at 244 m/s, as shown in Table 3, where compressible flow CFD should be used. For X/D of 6.54 and 4.66, Fig. 19a shows that there was very good agreement between the experimental and the CHT CFD results. Both the experiments and predictions showed the deterioration of h with the cross-flow, due to the downstream convection of the turbulence on the surface, as shown above and correlated in Eq. 7. This is in a region of X/D where flow-maldistribution was not significant. However, at lower X/D, as shown in Fig. 19b, the experimental results showed first a decrease in h with distance along the impingement gap, due to the cross-flow effect correlated by Eq. 7, and then an increase due to the influence of flow-maldistribution. This effect was reasonably well predicted using CHT CFD for an X/D of 3.76, although the leading and trailing edges were under predicted and the central section over predicted.

Finally, at the lowest X/D of 1.86 the experimental and predicted results were in agreement over a continuous increase in h from the start to end of the gap, due to the strong flow-maldistribution at this X/D with a very low impingement jet pressure loss. However, the predictions under predicted the experimental results at all axial positions. The difference was 50% at the start of the gap and 18% by hole 10. As discussed above in relation to the surface averaged h results, these results are difficult to explain as predicted h is higher than that measured would be expected, due to the location of the thermocouples on the centreline between the impingement holes.

Accepted Manuscript Not Copyedited

Downloaded From: http://turbomachinery.asmedigitalcollection.asme.org/ on 08/11/2014 Terms of Use: http://asme.org/terms

Journal of Turbomachinery. Received July 07, 2014;
Accepted manuscript posted August 11, 2014. doi:10.1115/1.4028232
Copyright (c) 2014 by ASME

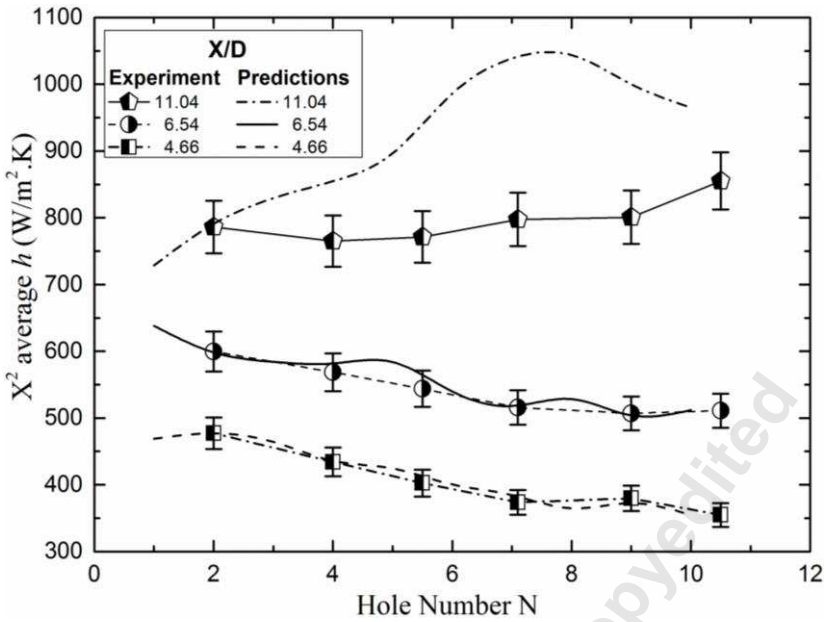

(a) Higher X/D

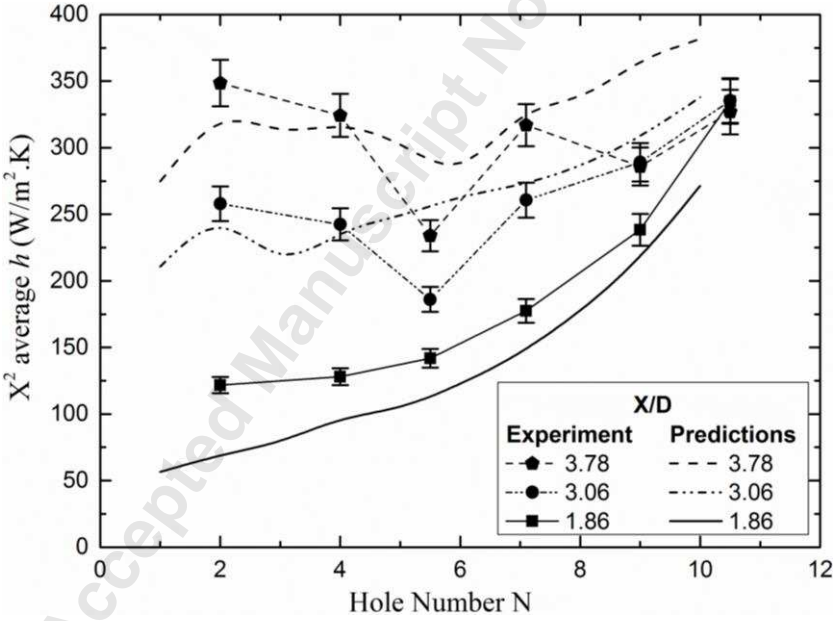

(b) Lower X/D

Fig.19: Comparison of target $\mathbf{X^2}$ average heat transfer coefficient h at constant mass velocity G of 1.93kg/sm^{2}bar

Downloaded From: http://turbomachinery.asmedigitalcollection.asme.org/ on 08/11/2014 Terms of Use: http://asme.org/terms

Journal of Turbomachinery. Received July 07, 2014;
Accepted manuscript posted August 11, 2014. doi:10.1115/1.4028232
Copyright (c) 2014 by ASME

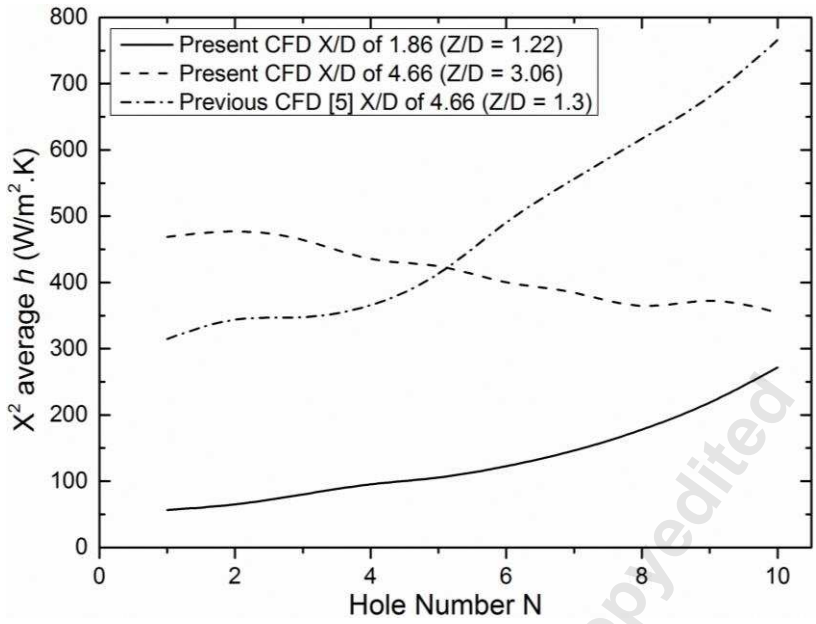

Fig.20: Comparison of predicted X^2 average h with previous CFD prediction showing influence of Z/D

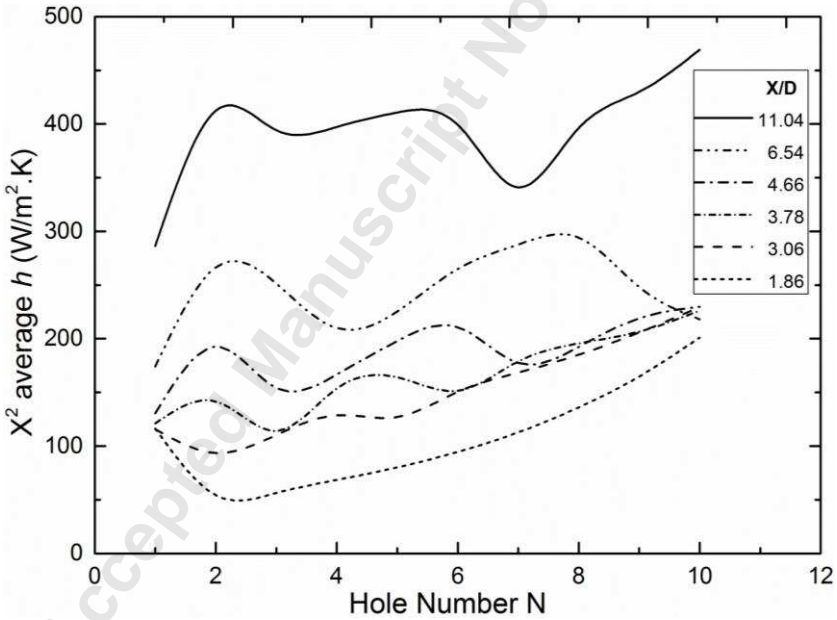

Fig.21: Prediction of X^2 average heat transfer coefficient h on the inside impingement wall surface at G of 1.93kg/sm^{2}bar

Accepted Manuscript Not Copyedited

Downloaded From: http://turbomachinery.asmedigitalcollection.asme.org/ on 08/11/2014 Terms of Use: http://asme.org/terms

Journal of Turbomachinery. Received July 07, 2014;
Accepted manuscript posted August 11, 2014. doi:10.1115/1.4028232
Copyright (c) 2014 by ASME

The prediction of the X/D of 1.86 in Fig. 13 showed very low TKE over the first few rows of holes, which was due to the very low predicted proportion of flow in these holes as shown in the very low predicted velocities in Fig. 9. The resultant predicted flow-maldistribution in Fig. 7 was severe with > 5 times the flow in row 10 to that in row 1. Table 3 gives the hole Re as 3850, based on the assumption of equal distribution of the air flow. However, the Re in the first row of holes with the predicted flow-maldistribution was 1540 and the applicability of the turbulent flow modelling under very low jet Re conditions is probably the main cause of the prediction errors for the X/D = 1.86 impingement geometry. Figure 20 investigates the consequences of the Z/D in the present work, when X/D is varied at constant Z of 10mm, which involves a variation of Z/D. The authors have previously investigated the CHT CFD predictions of the influence of Z at constant X/D of 4.66 [5], which are compared with the present work in Fig. 20. Figure 20 shows that for an X/D of 4.66 the effect of reducing Z to reduce Z/D was to increase the cross-flow induced flow-maldistribution, so that the axial variation in h along the impingement target wall was changed to a continuous increase with distance from a continuous decrease with distance. This was the main reason for the present work being undertaken at constant Z, which was considered a more practical design situation. The effect was to keep the cross-flow in the gap constant as X/D was varied. The comparison in Fig. 20 is for the X/D = 4.66 and Z/D = 3.06 or X/D = 1.86 and Z/D = 1.22 results with those of a similar Z/D in the previous work. This shows a similar proportionate influence of cross-flow. However, it is clear that the large difference in the magnitude of h at all axial positions was due to the X/D effect and not the Z/D variation in the present work at constant Z.

Predicted Axial Variation X^2 Local Average HTC on the Impingement Jet Surface along the Gap

The predicted results for the surface distribution of h on the bottom surface of the impingement jet wall in Fig. 18 were surface averaged on an X^2 basis and the axial variation of this is shown in Fig. 21. The most significant feature of the results is that for X/D of 4.66, 3.78 and 3.06, the predicted results showed an increased in h with axial distance. This contrasts directly with the decreased h along axial direction for the target surface of X/D = 4.66 in Fig. 19a. In the downstream portion of the impingement wall the X^2

Accepted Manuscript Not Copyedited

Downloaded From: http://turbomachinery.asmedigitalcollection.asme.org/ on 08/11/2014 Terms of Use: http://asme.org/terms

Journal of Turbomachinery. Received July 07, 2014;
Accepted manuscript posted August 11, 2014. doi:10.1115/1.4028232
Copyright (c) 2014 by ASME

averaged h was predicted to be 230W/m^{2}K for X/D 4.66, 3.78 and 3.06 compared with the target surface X^2 h of 350 for X/D 4.66, 370 for 3.78 and 340W/m^{2}K for 3.06.

As there have been no previous publications of the heat transfer to the impingement wall surface these predictions cannot be verified. However, the target surface predictions for X^2 average h were in good agreement with the measurements in Fig. 19, so the impingement jet surface predicted h would be concluded to be reasonable. These results indicate that heat transfer to this surface is a significant part of the overall impingement wall cooling performance. Under realistic hot wall conditions, the impingement jet wall would be heated and this would heat the impingement jet. Thus prediction of the performance of impingement cooling needs to know this impingement jet surface heat transfer.

The prediction of the target wall X^2 average h was not in good agreement with the measurements for X/D = 11.04 and 1.86, as shown in Fig.19a and b. Hence, the predictions of the impingement jet wall X^2 average h must be less reliable. Figure 18 shows that if the whole 10 rows of holes are surface averaged then the impingement jet wall h was about half of the target wall h. However, comparison of Figs. 19 and 21 shows that the axial variation of the ratio for X/D = 4.66 was 0.3 - 0.66 and this would have to be taken into account in predicted impingement cooling. For X/D = 6.54 that ratio of the initial and final h for the two surfaces was 0.3 and 0.45 and for X/D = 3.06 it was 0.4 and 0.7. Thus, there was predicted to be significant variation in the ratio of h between the two surfaces with X/D.

Distribution of Predicted Temperature

The present experimental results were undertaken with active electrical heating of the target wall. The CHT CFD predictions enabled the surface distribution of metal temperature in the presence of the impingement cooling to be predicted. The predicted results are in terms of the dimensionless temperature T* defined by Eq. 12. The use of the dimensionless temperature T* enables the present results to be applied to other higher temperature operations. The predicted surface distribution of T* is shown in Fig. 22. These plots are very similar in distribution to those for the distribution of Nu in Fig. 16, as expected.

$$T^* = \frac{(T - T_\infty)}{(T_w - T_\infty)} \qquad (12)$$

Accepted Manuscript Not Copyedited

Downloaded From: http://turbomachinery.asmedigitalcollection.asme.org/ on 08/11/2014 Terms of Use: http://asme.org/terms

Journal of Turbomachinery. Received July 07, 2014;
Accepted manuscript posted August 11, 2014. doi:10.1115/1.4028232
Copyright (c) 2014 by ASME

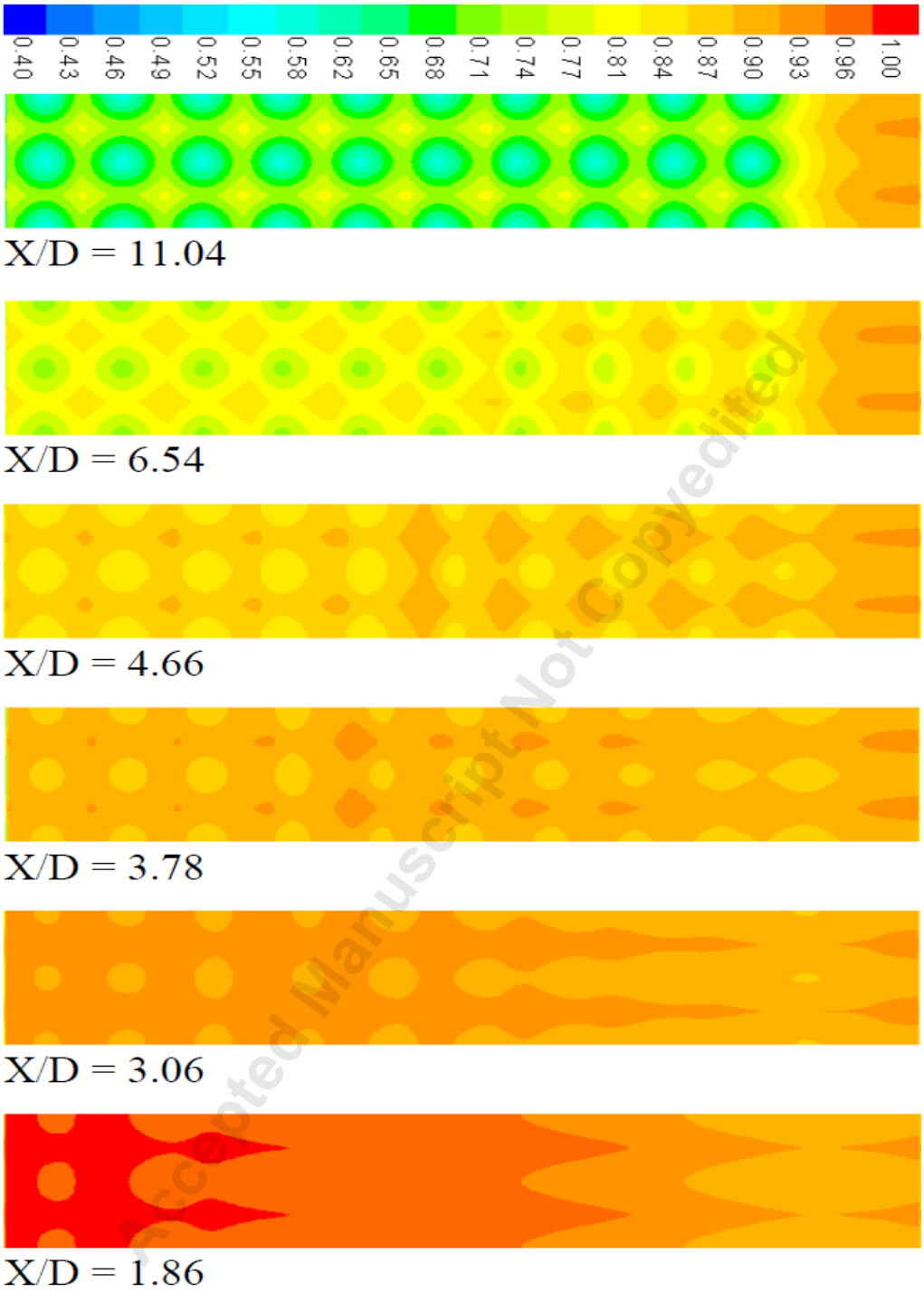

Fig. 22: Contours of normalized temperature on target wall surface for variable X/D at constant mass velocity G

Downloaded From: http://turbomachinery.asmedigitalcollection.asme.org/ on 08/11/2014 Terms of Use: http://asme.org/terms

Journal of Turbomachinery. Received July 07, 2014;
Accepted manuscript posted August 11, 2014. doi:10.1115/1.4028232
Copyright (c) 2014 by ASME

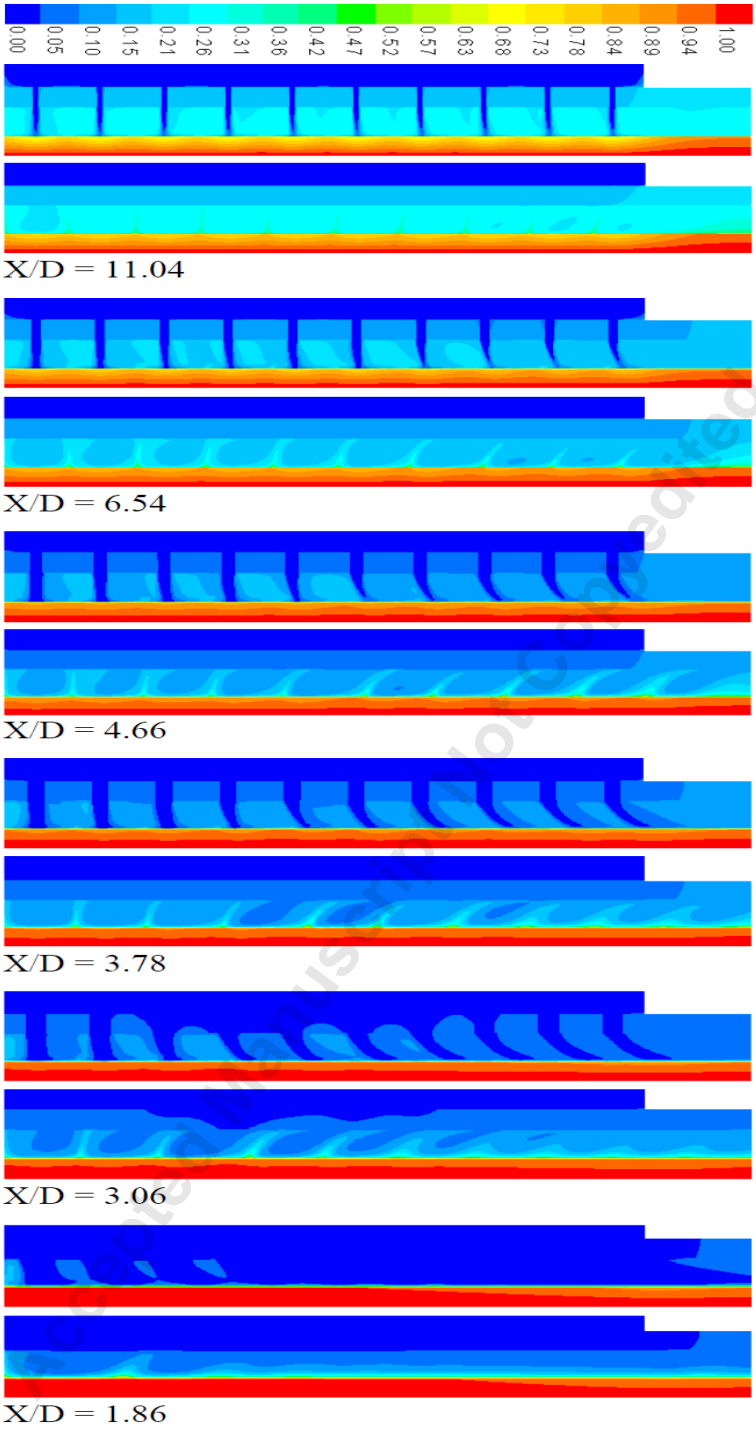

Fig. 23: Contours of normalized temperature in the impingement gap (in-line with and between N rows of holes) of variable X/D at constant mass velocity G

Downloaded From: http://turbomachinery.asmedigitalcollection.asme.org/ on 08/11/2014 Terms of Use: http://asme.org/terms

Journal of Turbomachinery. Received July 07, 2014;
Accepted manuscript posted August 11, 2014. doi:10.1115/1.4028232
Copyright (c) 2014 by ASME

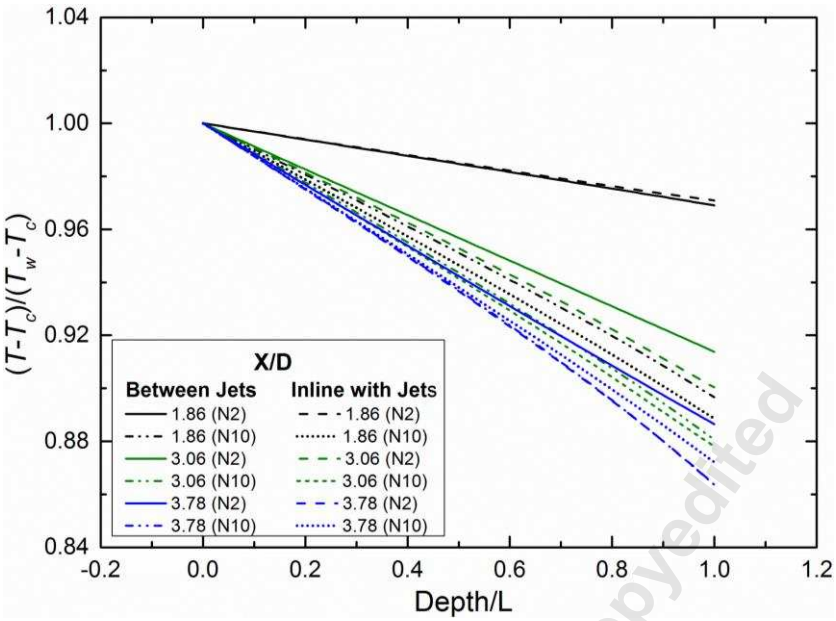

(a) Lower X/D

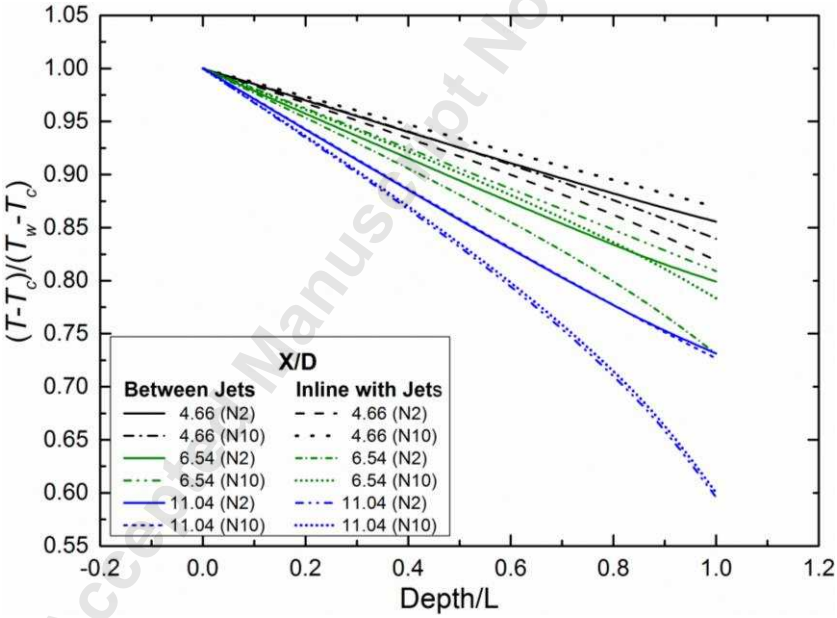

(b) Higher X/D

Fig.24: Lower X/D prediction of normalize temperature gradient in the target wall thickness of 6.35mm

Figure 22 shows the existence of significant thermal gradients, in spite of the internal heat conduction within the wall. However, the predicted temperature gradients are much lower than those for the local Nu

Downloaded From: http://turbomachinery.asmedigitalcollection.asme.org/ on 08/11/2014 Terms of Use: http://asme.org/terms

Journal of Turbomachinery. Received July 07, 2014;
Accepted manuscript posted August 11, 2014. doi:10.1115/1.4028232
Copyright (c) 2014 by ASME

gradients predicted in Fig. 16. For example, for X/D = 11.04, the Nu variation between the impingement point and the mid-distance between the impingement points is a factor of 10/1, but the same T* gradient is only about 1.5.

The Heating of the Impingement Cooling Air at the Hot Target Surface

A feature of hot wall impingement heat transfer is that the coolant jet is heated by the heat transfer at the surface. The heated jet has a reverse flow jet that impinges on the impingement jet surface and heats up the coolant jet. Figure 23 shows the contours of T* for the heated air in the impingement gap. For each X/D two 2D T* distributions are shown, one on the centreline of the impingement jets and the other on the midway between the rows of impingement jets, where the reverse flow jet occurs. Figure 23 clearly shows the presence of the reverse flow heated jet and its impingement on the impingement jet wall surface. There is also a strong deflection of the reverse flow jets by the cross-flow. For example, for X/D = 3.78 the deflection of the reverse flow jet results in the reverse flow jet from hole 8 occurring between the impingement jets at row 10. For an X/D of 6.54, the higher velocity impingement jets and the same cross-flow velocity results in the reverse jet from row 8 occurring between the impingement jets for row 9.

Thermal Gradients through the Wall Thickness

Figure 24 shows the dimensionless temperature distributions in the Nimonic-75 wall thickness. These are difficult to see on the scale of Fig. 23 and are plotted in Fig. 24 as T* as a function of the depth in the wall. The thermal gradient in Fig. 24, are for the in-line plane with the impingement jets and between the impingement jets for hole 2 and hole 10 for each range of X/D. The difference was small, indicating that the thermal gradients along the surface of the metal wall were small. Figure 23 show that the thermal gradients in the wall thickness were predicted to be much greater than those between the holes. This is because the computation holds the bottom side of the wall metal thickness at a fixed temperature. The authors [8] have shown that the thermal gradients along the surface between the impingement jet centreline were predicted to be much smaller than those through the metal thickness, which at the present G of 1.93kg/sm^{2}bar were about 2%. Figure 24 shows as expected that the higher the heat transfer the greater the

Accepted Manuscript Not Copyedited

Downloaded From: http://turbomachinery.asmedigitalcollection.asme.org/ on 08/11/2014 Terms of Use: http://asme.org/terms

Journal of Turbomachinery. Received July 07, 2014;
Accepted manuscript posted August 11, 2014. doi:10.1115/1.4028232
Copyright (c) 2014 by ASME

thermal gradients in the wall. Thus, the thermal gradients were predicted to be lowest at low X/D and highest at high X/D.

CONCLUSIONS

Experimental results for impingement cooling were presented for a G of 1.93 kg/sm^{2}bar for the locally surfaced averaged heat transfer coefficient h. The impingement jet and target metal walls were Nimonic-75 of 6.35mm metal thickness. Square array impingement jets were investigated for a range of X/D which was varied by changing the hole diameter D at constant pitch X and Z. The impingement flow pressure loss ΔP/P was also measured for a constant G (1.93kg/sm^{2}bar). These results were compared with CHT CFD predictions at the same G, which is typical of the total compressor exit mass flux used to regeneratively cool a combustor wall.

The X^2 averaged heat transfer coefficients h were very well predicted for X/D of 6.54 and 4.66, which are in the region commonly used in impingement heat transfer. The CHT CFD predictions agreed with the experiments in the predicted pressure loss and in the deterioration of the heat transfer with axial distance due to the impact of the cross-flow. For X/D of 3.78 and 3.06 the agreement with experimental pressure loss was good, but there was less satisfactory agreement with the X^2 averaged axial variation of h. The predictions gave an axial variation of h that was less than that observed, although the total surface averaged h showed good agreement with the experimental results.

For an X/D of 11.04 the agreement with the pressure loss measurements was good, but the prediction of h was too high and the axial variation of h was predicted to increase with distance along the impingement gap, while the experiments showed a more uniform distribution in h. It is considered that the very high impingement jet velocities at this X/D and high G would require compressible flow CFD computations, the present incompressible flow predictions were probably inadequate.

For an X/D of 1.86, the predictions were low for pressure loss and low for h, although the axial variation of h was predicted to be similar to that measured. Laminar flow occurred in the first few rows of holes, which was not taken into account in the predictions.

Accepted Manuscript Not Copyedited

Downloaded From: http://turbomachinery.asmedigitalcollection.asme.org/ on 08/11/2014 Terms of Use: http://asme.org/terms

Journal of Turbomachinery. Received July 07, 2014;
Accepted manuscript posted August 11, 2014. doi:10.1115/1.4028232
Copyright (c) 2014 by ASME

The CHT CFD predictions enabled the heat transfer to the impingement jet wall to be predicted. On average this h was about 50% of that for the impingement target wall at all X/D. However, there were significant variations in this ratio with X/D and between the first few holes and the last few holes.

The thermal gradients in the metal wall were much greater through the thickness of the wall than the axial gradients between the jet impingement points. These gradients increased as the heat transfer coefficient increased and were greatest at the highest X/D.

Conjugate heat transfer CFD has been shown to give good predictions of impingement cooling and is a viable design tool for combustor and turbine blade cooling design.

ACKNOWLEDGEMENTS

Abubakar M. El-jummah wishes to acknowledge the financial support from University of Maiduguri and the Government of Nigeria. The experimental work was supported by EPSRC research grants and the test walls were supplied by Siemens Turbomachinery.

NOMENCLATURE

A Impingement hole porosity = $[(\pi/4)D^2]/X^2$

D Impingement air hole diameter, m

C_d Discharge coefficient

G Coolant mass flux, kg/sm^{2}bar

G_1 First upstream rows of holes coolant G, kg/sm^{2}bar

G_c Cross-flow mass flow/unit area, kg/sm^{2}bar

G_N Coolant G for N upstream rows of holes, kg/sm^{2}bar

h Heat transfer coefficient (HTC), W/m^{2}K

I_C Cross-flow interference parameter

k_f Thermal conductivity of fluid, W/mK

L Target wall metal thickness, m

n Number of impingement hole/unit surface area, m^{-2}

N Number of upstream rows of impingement holes

Accepted Manuscript Not Copyedited

Downloaded From: http://turbomachinery.asmedigitalcollection.asme.org/ on 08/11/2014 Terms of Use: http://asme.org/terms

Journal of Turbomachinery. Received July 07, 2014;
Accepted manuscript posted August 11, 2014. doi:10.1115/1.4028232
Copyright (c) 2014 by ASME

Nu	Nusselt Number
Nu_o	Nusselt number with zero crossflow
ρ	Density of air, kg/m^3
ΔP	Impingement wall pressure loss, Pa
P	Coolant supply static pressure (approx. 1bar)
Pr	Prandtl number
q"	Heat flux on the target wall, W/m^2
R	Gas constant for air, 287 J/kg.K
Re_h	Impingement hole Reynolds number (V_jD/ν)
T_∞	Coolant temperature, 288K
T^*	Normalized mean temperature
T_w	Target wall imposed temperature (353K)
T_S	Target surface metal temperature, K
U_c	Impingement gap cross flow velocity at hole N, m/s
Uτ	Friction velocity $(\tau_w/\rho)^{0.5}$, m/s
τ_w	Wall shear stress, kg/ms^2
μ	Dynamic viscosity, kg/ms
V_j	Impingement jet mean velocity (or V_m), m/s
ν	Kinematic viscosity, m^2/s
W	Target wall total cooled length, m
dx	differential distance from the leading edge, m
X	Impingement hole square array pitch, m
y	Dimensionless pressure loss ratio
y^+	Inner variable wall normal coordinate ($\xi U\tau/\nu$)
Z	Impingement gap, m
ξ	Grid cell size, m

Accepted Manuscript Not Copyedited

Downloaded From: http://turbomachinery.asmedigitalcollection.asme.org/ on 08/11/2014 Terms of Use: http://asme.org/terms

Journal of Turbomachinery. Received July 07, 2014;
Accepted manuscript posted August 11, 2014. doi:10.1115/1.4028232
Copyright (c) 2014 by ASME

Subscripts

c Cross-flow

d Discharge

h Hole

j Jet

s Surface

w Wall

∞ Coolant

REFERENCES

[1] Andrews, G. E. and Hussain, C. I. 1984: "Impingement Cooling of Gas Turbine Components." High Temperature Technology: Butterworth & Co Publisher Ltd., Vol. 2 (2), 99 - 106.

[2] Obot, N. T. and Trabold, T. A. 1987, "Impingement Heat Transfer within Arrays of Circular Jets: Part 1-Efects of Minimum, Intermediate and Complete Crossflow for Small and Large Spacings." Trans. ASME J. Heat Transfer, Vol. 109, 872 - 879.

[3] Facchini, B. and Surace, M. 2006: "Impingement Cooling for Modern Combustors: Experimental Analysis of Heat Transfer and Effectiveness." Springer-Verlag J. Experiments in Fluids 40, 601- 611.

[4] El-jummah, A. M., Andrews, G. E., and Staggs, J. E. J. 2013: "Conjugate Heat Transfer CFD Predictions of Impingement Jet Array Flat Wall Cooling Aerodynamics with Single Sided Flow Exit." Proc. ASME GT2013-95343, pp. 1 - 12.

[5] El-jummah, A. M., Andrews, G. E., and Staggs, J. E. J. 2013: "Conjugate Heat Transfer CFD Predictions of the Influence of the Impingement Gap on the Effect of Crossflow." Proc. ASME HT2013-17180, pp. 1-12.

[6] Ito, E., Okada, I., Tsukagoshi, K., Muyama, A., and Masada, J. 2009: "Development of Key Technologies for the next Generation 1700C-Class Gas Turbine." Proc ASME Turbo Expo: Power for Land Sea and Air. Orlando, Florida GT2009-59783. pp. 1 – 11.

[7] Abdul Husain, R. A. A. and Andrews, G. E. 1990: "Full Coverage Impingement Heat Transfer at High Temperature." ASME 90-GT-285. pp. 1 - 12.

Accepted Manuscript Not Copyedited

Downloaded From: http://turbomachinery.asmedigitalcollection.asme.org/ on 08/11/2014 Terms of Use: http://asme.org/terms

Journal of Turbomachinery. Received July 07, 2014;
Accepted manuscript posted August 11, 2014. doi:10.1115/1.4028232
Copyright (c) 2014 by ASME

[8] El-jummah, A. M., Abdul Hussain, R. A. A., Andrews, G. E., and Staggs, J. E. J. 2013: "Conjugate Heat Transfer CFD Predictions of the Surface Averaged Impingement Heat Transfer Coefficients for Impingement Cooling with Backside Cross-flow." Proc. ASME IMECE2013-63580, pp. 1 - 12

[9] Abdul Husain, R. A. A., Andrews, G. E., Asere, A. A., and Ndiema, C. K. W. 1988: "Full Coverage Impingement Heat Transfer: Cooling Effectiveness." Proc. ASME 88-GT-270. pp. 1 - 9.

[10] Andrews, G. E. and Hussain, C. I. 1986: "Full Coverage Impingement Heat Transfer: Influence of Channel Height." Proc. 8th International Heat Transfer: Hemisphere Pub. Corp., pp. 1205 - 1211.

[11] Andrews, G. E. and Hussain, C. I. 1987: "Full Coverage Impingement Heat Transfer: The Influence of Crossflow." AIAA-87-2010, pp. 1 - 9.

[12] Andrews, G. E., Asere, A. A., Hussain, C. I., and Mkpadi, M. C. 1985: "Full Coverage Impingement Heat Transfer: The Variation in Pitch to Diameter Ratio at a Constant Gap." Proportion and Energetics Panel of AGARD, 65th Symposium 'Heat Transfer and Cooling in Gas Turbines' Paper 26, pp. 1 - 12.

[13] Andrews, G. E. and Hussain, C. I. 1984: "Full Coverage Impingement Heat Transfer: The Influence of Impingement Jet Size." 1st UK National Heat Transfer Conference, IChemE Symposium Series: No. 86, pp. 1115 - 1124.

[14] Chance, J. L. 1974: "Experimental Investigation of Air Impingement Heat Transfer under an Array of Round Jets." Tappi Vol. 57 (6), 108 - 112.

[15] Kercher, D. M. and Tabakoff, W. 1970: "Heat Transfer by a Square Array of Round Air Jets Impinging Perpendicular to a Flat Surface including Effects of Spent Air. "Trans. ASME J. Eng. Power, 63-GT-4, 73 - 82.

[16] Metzger, D. E. and Korstad, R. J. 1972: "Effects of Crossflow on Impingement Heat Transfer." Trans. ASME J. Eng. Power, 71-GT-1, 35-41.

[17] Florschuetz, L. W., Truman, C. R., and Metzger, D. E. 1981: "Streamwise Flow and Heat Transfer Distributions for Jet Array Impingement with Cross-flow." ASME, J. Heat Transfer, Vol. 103, 337 - 342.

Accepted Manuscript Not Copyedited

Downloaded From: http://turbomachinery.asmedigitalcollection.asme.org/ on 08/11/2014 Terms of Use: http://asme.org/terms

Journal of Turbomachinery. Received July 07, 2014;
Accepted manuscript posted August 11, 2014. doi:10.1115/1.4028232
Copyright (c) 2014 by ASME

[18] Bailey, J. C., Intile J., Fric, T. F., Tolpadi, A. K., Nirmalan, N. V., and Bunker, R. S. 2003: "Experimental and Numerical Study of Heat Transfer in a Gas Turbine Combustor Liner," Tran. ASME J. Eng. Gas Turbines and Power, Vol. 125, 994 - 1002.

[19] El-jummah, A. M., Abdul Hussain, R. A. A., Andrews, G. E., and Staggs, J. E. J. 2014: "Conjugate Heat Transfer CFD Predictions of Impingement Heat Transfer: Influence of Number of Holes for a Constant Pitch-to-Diameter Ratio X/D." Proc. ASME GT2014-25268, pp. 1 - 14

[20] Xing, Y., Spring, S. and Weigand, B. 2010: "Experimental and Numerical Investigation of Heat Transfer Characteristics of Inline and Staggared Arrays of Impinging Jets." Trans. ASME J. Heat Transfer, Vol. 132, 1-11.

[21] Hale, A. C., Plesniak, W. M. and Ramadhyani, S. 2000: "Structural Features and Surface Heat Transfer Associated with a Row of Short-Hole Jets in Cross-flow." Int. J. Heat and Fluid Flow, Vol. 21, 542 - 553.

[22] Nuutinen, M., Kaario, O. and Larmi, M. 2009: "Advances in Variable Density Wall Functions for Turbulent Flow CFD-Simulations, Emphasis on Heat Transfer." SAE International, 2009-01-1975, 1 - 16.

[23] Taslim, M. E. and Bethka, D. 2009: " Experimental and Numerical Impingement Heat Transfer in an Airfoil Leading-Edge Cooling Channel with Cross-flow." Trans. ASME, J. Turbomachinery, Vol. 131, 1 - 7.

[24] ASME V & V 20-2009: "Standard for Verification and Validation in Computational Fluid Dynamics and Heat Transfer." American Society of Mechanical Engineers.

[25] Bailey, J. C. and Bunker, R. S. 2002: "Local Heat Transfer and Flow Distributions for Impinging Jet Arrays of Dense and Sparse Extent." ASME GT-30473, pp. 1 - 10.

[26] Zhang, C., Wang, Z., Liu, J and An, B. 2013: "The Effects Biot Number on the Conjugate Film Cooling Effectiveness Under Different Blowing Ratios." ASME GT-94041, pp. 1 - 9.

[27] Johnson, J. J., King, P. I., Ni, R. H., Humber, W. and Clark, J. P. 2013: "Conjugate CFD Simulations of an Optimized Turbine Vane Film Cooling Array on Flat Plate Models." ASME GT-94383, pp. 1 - 11.

Accepted Manuscript Not Copyedited

Downloaded From: http://turbomachinery.asmedigitalcollection.asme.org/ on 08/11/2014 Terms of Use: http://asme.org/terms

Journal of Turbomachinery. Received July 07, 2014;
Accepted manuscript posted August 11, 2014. doi:10.1115/1.4028232
Copyright (c) 2014 by ASME

[28] Lad, B. and He, L. 2013: "An Immersed Mesh Block (IMB) Approach for Conjugate Heat Transfer Predictions." ASME GT-94053, pp. 1 - 12.

[29] Panda, R. K. and Prasad, B. V. S. S. S. 2012: "Conjugate Heat Transfer from Flat Plate with Combined Impingement and Film Cooling." ASME GT-68830, pp. 1 - 10.

[30] Sidwell, T. G., Lawson, S. A., Straub, D. L., Casleton, K. H. and Beer, S. 2013: "Conjugate Heat Transfer Modelling of a Film-Cooled, Flat-Plate Test Specimen in a Gas Turbine Aero thermal Test Facility." ASME GT-94687, pp. 1 - 16.

[31] Lawson, S. A., Straub, D. L., Beer, S., Casleton, K. H., and Sidwell, T. G. 2013: "Direct Measurement of Overall Effectiveness and Heat Flux on a Film Cooled Test Article at High Temperatures and Pressures." ASME GT-94685, pp. 1 - 12.

[32] Hao, Z., Ren, X., Song, Y., and Gu, C. 2013: "An Investigation of Conjugate Heat Transfer Simulations Based on Discontinuous Galerkin Methods on Unstructured Grids." ASME GT-94498, pp. 1 - 12.

[33] Ni, R., Clark, J. P., Humber, W., Anthony, R. J., Fan, G., and Johnson, J. J. 2013: "Comparison of Predictions from Conjugate Heat Transfer Analysis of a Film-Cooled Turbine Vane to Experimental Data." ASME GT-94716, pp. 1 - 13.

[34] Oguntade, H. I., Andrews, G. E., Burns, A., Ingham, D. and Pourkashanian, M. 2011: "Predictions of Effusion Cooling with Conjugate Heat Transfer." ASME GT-45517.

[35] Oguntade, H.I., Andrews, G.E., Ingham, D.B., Burns, A.D. and Pourkashanian, M. 2012: "Conjugate Heat Transfer Predictions of Effusion Cooling: The Influence of the Coolant Jet Flow Direction on the Cooling Effectiveness." ASME GT-68517.

[36] Oguntade, H.I., Andrews, G.E., Ingham, D.B., Burns, A.D. and Pourkashanian, M. 2012: "Conjugate Heat Transfer Predictions of Effusion Cooling: The Influence of the Injection Hole Size on Cooling Performance. ASME GT-68516, pp. 1 - 14.

Accepted Manuscript Not Copyedited

Downloaded From: http://turbomachinery.asmedigitalcollection.asme.org/ on 08/11/2014 Terms of Use: http://asme.org/terms